Insights into Early Earth from the Pt-Re-Os isotope and Highly Siderophile Element abundance systematics of Barberton komatiites

Igor S. Puchtel[1], Richard J. Walker[1], Mathieu Touboul[1],
Euan G. Nisbet[2], and Gary R. Byerly[3]

[1]Department of Geology, University of Maryland, 237 Regents Drive, College Park, MD 20742, USA
[2]Department of Earth Sciences, Royal Holloway, University of London, Egham TW20 0EX, UK
[3]Department of Geology and Geophysics, Louisiana State University, Baton Rouge, LA 70803, USA

Corresponding author:
Igor S. Puchtel
e-mail: ipuchtel@umd.edu

Submitted to:
Geochimica et Cosmochimica Acta
Version 2013/05/08

Abstract

Platinum-Re-Os isotopic and highly siderophile element (HSE: Os, Ir, Ru, Pt, Pd, and Re) abundance data are reported for well-preserved komatiites from the Komati and Weltevreden Formations of the Barberton Greenstone Belt, South Africa. The Re-Os data for whole-rock samples and olivine and chromite separates define isochrons with ages of 3484±38 and 3263±12 Ma for the Komati and Weltevreden systems, respectively. The respective initial $^{187}Os/^{188}Os$ = 0.10335±15 ($\gamma^{187}Os$ = +0.34±0.15) and 0.10442±4 ($\gamma^{187}Os$ = -0.14±0.04) are within the chondritic range. When considered together with the Re-Os data for late Archean komatiite systems, these data indicate that the mantle sources of most Archean komatiites evolved with essentially chondritic long-term Re/Os. By contrast, the initial $^{186}Os/^{188}Os$ = 0.1198283±9 ($\varepsilon^{186}Os$ = -0.12±0.08) and 0.1198330±8 ($\varepsilon^{186}Os$ = +0.22±0.07) for the Komati and Weltevreden systems, respectively, are non-chondritic, indicating that the mantle sources of these two komatiite systems evolved with fractionated time-integrated Pt/Os. These new $^{186,187}Os$ isotopic data for the early Archean komatiite systems, combined with published $^{142,143}Nd$ and ^{176}Hf isotopic data for the same rocks, are consistent with formation and long-term isolation of deep-seated mantle domains with fractionated time-integrated Sm/Nd, Lu/Hf, and Pt/Os ratios, at ca. 4400 Ma. These domains may have been generated as a result of late-stage crystallization of a primordial magma ocean involving Mg-perovskite, Ca-perovskite and Fe-Pt alloys acting as the fractionating phases. The inferred mantle domains were sampled by the early Archean komatiites, but were largely mixed away by 2.7 Ga, as evidenced by uniform, time-integrated Sm/Nd, Lu/Hf, and Pt/Os ratios inferred for the sources of most late Archean komatiite systems. The total Pt and Pd abundances present in the sources of the early Archean komatiite systems are calculated to be between 60-70% of those present in the estimates for the modern primitive mantle. These are within the range of the total Pt and Pd abundances present in the sources of late Archean komatiite systems, indicating little change in the HSE abundances in the Archean mantle between 3.5 and 2.7 Ga. The new HSE data for the early Archean komatiite systems may implicate late accretion of HSE to the mantle prior to completion of crystallization of a final terrestrial magma ocean, followed by sluggish mixing of diverse post-magma ocean domains, characterized by variably fractionated lithophile element and HSE abundances.

Keywords: Barberton Greenstone Belt, Komati and Weltevreden komatiites, Highly Siderophile Elements, Re-Os and Pt-Os isotope systematics, late accretion, terrestrial magma ocean.

1. Introduction

Precisely determining the absolute and relative abundances of the highly siderophile elements (HSE; including Re, Os, Ir, Ru, Pt, and Pd) in the early terrestrial mantle is crucial for understanding such fundamental planetary processes as the Earth's primary separation of metallic core from silicate mantle (Righter, 2003), continued accretion following core formation (Morgan et al., 1981; Morgan, 1985, 1986; Walker, 2009), differentiation of the mantle (Walker et al., 1989), recycling of oceanic lithosphere (Walker et al., 1991; Hauri and Hart, 1993; Lassiter and Hauri, 1998), mass transfer in subduction zones (Brandon et al., 1996; Alves et al., 1999; Brandon et al., 1999; Woodland et al., 2002; Penniston-Dorland et al., 2012), and, possibly, inner core crystallization and core-mantle exchange (Walker et al., 1995; Brandon et al., 1998; Puchtel and Humayun, 2000; Puchtel et al., 2005).

The absolute HSE abundances and initial $^{186,187}Os/^{188}Os$, that reflect the time-integrated Pt/Os and Re/Os in mantle domains, have previously mainly been estimated for relatively recent upper mantle via studies of ophiolites, abyssal peridotites, orogenic lherzolites, and mantle xenoliths representing subcontinental lithospheric mantle (Morgan et al., 1981; Morgan, 1986; Snow and Reisberg, 1995; Rehkämper et al., 1997; Handler and Bennett, 1999; Brandon et al., 2000; Meisel et al., 2001; Walker et al., 2002; Luguet et al., 2003; Pearson et al., 2004; Becker et al., 2006; Luguet et al., 2007; Liu et al., 2009; Fischer-Gödde et al., 2011). Most Re-Os isotopic data for young mantle materials and mantle-derived lavas suggest that the convecting upper mantle,

on average, has evolved with Re/Os broadly within the range of chondritic meteorites (Walker, 2009). The more limited Pt-Os isotopic data are likewise consistent with the average mantle bearing a long-term Pt/Os within the range of chondritic meteorites (Walker et al., 1997; Brandon et al., 2000; Brandon et al., 2005b). Finally, the relative abundances of other HSE in primitive mantle (PM) estimates have been shown to be either within or slightly outside the range defined by chondritic meteorites (Becker et al., 2006; Fischer-Gödde et al., 2011).

Most mantle materials that have been studied for HSE and Os isotopic compositions, however, have been heavily processed via melt extraction, crystal-liquid fractionation events and fluid- or melt-rock interactions, the effects of which have often made it problematic to constrain the HSE abundances in their respective mantle domains (e.g., Rehkämper et al., 1999a; Rehkämper et al., 1999b; Becker et al., 2006; Lorand et al., 2009). In addition, these young materials do not provide direct information about the HSE systematics of the Archean mantle, which is the key to understanding the early stages of the Earth's evolution. The study of komatiites can potentially circumvent some of these issues. Most komatiites likely formed via high degrees of partial melting of mantle materials on ascent (e.g., Arndt, 1977; Arndt et al., 2008), leading to the extraction of large proportions of the HSE from their mantle sources (Barnes et al., 1985; Keays, 1995; Rehkämper et al., 1999b). High degree mantle melting provides a mechanism for obtaining representative samples of large mantle domains that is not possible with small, individual mantle samples, or lower degree melts. Because komatiitic magmas are superheated, have low viscosities, and ascend rapidly (Huppert and Sparks, 1985), they undergo little to no differentiation prior to emplacement. The relatively high abundances of HSE in komatiitic liquids also make their HSE less prone to modification by crustal contamination. Further, Archean komatiites provide information about the abundances of HSE in

the mantle at a time when it, undoubtedly, was less modified by processes of melt extraction and re-fertilization, compared to the modern mantle. Finally, differentiation of komatiite lavas usually leads to fractionation of Os from Pt and Re. The resulting range in Re/Os and Pt/Os ratios among different portions of lava flows permits generation of isochrons, which can be used to obtain precise geochronological information, assess closed-system behavior of the HSE, and precisely determine initial Os isotopic compositions and time-integrated Re/Os and Pt/Os in the sources of the lavas. Typical correlations between MgO and HSE, combined with Os isotopic data, can also be used to precisely calculate absolute HSE abundances in the sources of komatiite lavas (Puchtel et al., 2004b; Puchtel and Humayun, 2005; Puchtel et al., 2007; Puchtel et al., 2009a; Puchtel et al., 2009b).

Some 25 years ago, the first terrestrial Re-Os isochron, on the 2.7 Ga Pyke Hill komatiites (Walker et al., 1988), and the first HSE abundance data, on the 2.7 Ga Abitibi and 89 Ma Gorgona komatiites (Crocket and MacRae, 1986; Brügmann et al., 1987), were published. Since then, following major advances in analytical techniques, a large body of Os isotopic and HSE abundance data on Archean and post-Archean komatiite systems has accumulated (e.g., Barnes et al., 1985; Walker et al., 1991; Shirey et al., 1994; Foster et al., 1996; Shirey, 1997; Walker et al., 1997; Rehkämper et al., 1999b; Walker et al., 1999; Walker and Stone, 2001; Bennett et al., 2002; Gangopadhyay and Walker, 2003; Maier et al., 2003; Wilson et al., 2003; Hanski et al., 2004; Gangopadhyay et al., 2005; Gangopadhyay et al., 2006; Maier et al., 2009; Fiorentini et al., 2011). However, despite these very substantial advances, the number of studies of Archean komatiitic systems that include complete sets of complementary HSE abundance and Pt-Re-Os isotopic data, as well as lithophile trace element and isotopic data, on pristine mantle lavas, remains limited. This database currently includes only a handful of late Archean localities, such

129 as the 2.9 Ga Sumozero-Kenozero (Puchtel et al., 2007), 2.8 Ga Kostomuksha (Puchtel et al.,
130 1998; Puchtel et al., 2005; Puchtel and Humayun, 2005), the 2.7 Ga Abitibi and Belingwe
131 (Puchtel et al., 2004a; Puchtel et al., 2004b; Puchtel et al., 2009b) and the 2.4 Ga Vetreny Belt
132 (Puchtel et al., 2001b; Puchtel and Humayun, 2001) komatiite systems. The early Archean record
133 is incomplete at best, with only two komatiite systems, the 3.55 Ga Schapenburg Greenstone
134 Remnant (Puchtel et al., 2009a) and the 3.26 Ga Weltevreden Formation (Connolly et al., 2011),
135 both of the Barberton Greenstone Belt (BGB) in South Africa, studied to date. This is due in part
136 to the poor state of preservation of the early Archean geological record in general, and the
137 komatiite record in particular, and in part to the extreme analytical challenges that this type of
138 study poses.

139 Komatiites of the BGB, which represents the type locality of the class of rock (Viljoen and
140 Viljoen, 1969), provide a particularly valuable source of information about the HSE systematics
141 of the early Archean mantle. First, these are the oldest recognizable komatiites on Earth, some of
142 which are also characterized by a good state of preservation of their original, magmatic features.
143 Second, these komatiites have unusual chemical compositions, including extremely high MgO
144 contents of the emplaced lavas and variable depletions/enrichments in Al and heavy rare earth
145 elements (REE). These chemical features clearly distinguish them from younger komatiites and
146 imply very specific conditions for their magma generation that apparently ceased to exist by the
147 late Archean. Third, the BGB contains a *ca.* 300 Ma record of evolution of komatiite
148 magmatism; this provides a unique opportunity to track secular changes in the absolute and
149 relative HSE abundances in the Archean mantle.

150 Here, we report HSE abundance and Re-Os and Pt-Os isotopic data for well-preserved
151 komatiites from the 3.48 Ga Komati Formation (Fm.) of the Barberton Greenstone Belt (BGB) in

South Africa. We also report Pt-Os isotopic data, as well as additional HSE abundance and Re-Os isotopic data to those reported by Connolly et al. (2011), for the 3.26 Ga Weltevreden Fm. of the BGB. These early Archean komatiite systems, together with the 3.55 Ga Schapenburg system studied by Puchtel et al. (2009a), are particularly interesting with respect to early Earth evolution in that they formed at a time when it has been speculated that HSE abundances in the komatiites were increasing due to the simple downward mixing of a veneer of HSE-rich materials added to Earth by late accretion (Maier et al., 2009; Fiorentini et al., 2010).

New data reported here are used to reconstruct the absolute and relative HSE abundances in the early Archean mantle, and to discuss implications for early terrestrial accretion history in view of these data, combined with the lithophile trace element and isotope systematics for these (Puchtel et al., 2013), as well as the HSE systematics for the well-studied late Archean komatiite systems.

2. Geological background and sampling

The BGB is located in the Kaapvaal Craton, one of the best preserved areas of pristine Archean crust on Earth, and consists of a succession of supracrustal rocks, ranging in age from 3.55 to 3.22 Ga, that make up three main lithostratigraphic units of ~15 km in total thickness: the lower, mostly volcanic, Onverwacht Group, and the upper, predominantly sedimentary, Fig Tree and Moodies Groups (Lowe, 1994, 1999; Lowe and Byerly, 1999, 2007). The Onverwacht Group includes several formations; komatiites from the Komati and Weltevreden Fms. are the subject of this study. The age of the Komati Fm. was determined to be 3482±5 Ma using the U-Pb zircon method on a thin layer of dacitic tuff (Armstrong et al., 1990). The emplacement age

of the komatiitic lavas from the Weltevreden Fm. was recently directly determined to be 3266±8 Ma using the Re-Os geochronometer (Connolly et al., 2011).

The Komati Fm. is divided into lower (1.8 km thick) and upper (1.3 km thick) members, with komatiites dominating the Lower Komati, and komatiitic basalts being prevalent in the Upper Komati (Viljoen et al., 1983; Dann, 2000). Abundances of some HSE in the Komati Fm. komatiites were previously reported by Maier et al. (2003). The absolute HSE abundances were found to be relatively low, which was attributed by these authors to the retention of the HSE in sulfides in the mantle source region. The HSE abundances were also found to plot with significant scatter on HSE vs. MgO variation diagrams, which was interpreted by Maier et al. (2003) to indicate HSE mobility during seafloor alteration and metamorphism.

Hand specimens for this study were collected from the Lower Komati Fm., in the type area, at the hillcrest of the locality illustrated by Viljoen et al. (1983) in their Fig. 3, and by Viljoen and Viljoen (1969), also in their Fig. 3. At this well-exposed and locally near-continuous 120 m section, a sequence of differentiated komatiite lava flows, ranging in thickness from <1 m to >10 m, was identified. Fifteen whole-rock samples (plus multiple replicates) and olivine and chromite separates were analyzed for HSE abundances and Pt-Os and Re-Os isotopic systematics. For the whole-rock samples, we utilized the same sample powder aliquots studied by Puchtel et al. (2013) for lithophile trace element and isotope systematics (see Fig. 1 in Puchtel et al. (2013) for sample locations).

The Weltevreden Fm. is located in the northern facies of the BGB. It accumulated as a thick sequence of komatiitic and basaltic volcanic rocks, komatiitic tuffs, and ultramafic intrusions (Lowe and Byerly, 1999). The exact thickness of the Weltevreden Fm. is unknown, but at least a few thousand meters of section are present, with individual flow units being 10 to 500 m thick

(Lowe and Byerly, 1999). The initial Re-Os isotopic and HSE abundance data for the Weltevreden Fm. komatiites were reported by Connolly et al. (2011).

For this study, we again used the sample powder aliquots utilized in the Puchtel et al. (2013) study. These samples were collected from three differentiated komatiite lava flows, SA501, KBA12, and SA564, which are ~65 m-, 25 m-, and 23 m thick, respectively (see Fig. 2 in Puchtel et al. (2013) for sample locations). Although all lava flows generally exhibit a classic layered structure similar to that in the lava flows from the Komati Fm. type locality, the spinifex zones are very thin, with the bulk of the lava flows consisting of cumulate komatiite. The details of the field petrology and petrography have been reported in Kareem (2005), Connolly et al. (2011) and Stiegler et al. (2012).

3. Analytical techniques

3.1. Sample preparation and mineral separation

The procedures for sample preparation closely followed those described in detail by Puchtel et al. (2009a) and Puchtel et al. (2009b). Hand specimens of 0.5-2 kg were collected from surface outcrops and cut into 1-2 cm thick slabs using a diamond saw to remove any signs of alteration. Small pieces were cut off the slabs and used to prepare polished thin sections at the Institute of Geology of Ore Deposits (IGEM) in Moscow. The remaining parts of the slabs were polished on all sides using SiC sandpaper to remove saw marks, washed in de-ionized water, dried, and crushed in an alumina-faced jaw crusher. A 200-g aliquot of crushed sample was pre-ground in an alumina shatter box, then ground to a fine powder in an alumina-faced disk mill and used for the geochemical studies. The remaining crushes of the largest available and freshest samples, including BV03 and BV10 (Komati Fm.) and 501-1, 501-8, and 12-6 (Weltevreden Fm.) were used for mineral separation. Pure olivine and chromite separates were obtained at the Institute of Geology in Petrozavodsk using the combination of heavy liquid and magnetic separation techniques and handpicking.

3.2. Highly siderophile elements

3.2.1 Re-Os isotopic and HSE abundance data. To obtain the Re-Os isotopic and HSE abundance data, 1.3-1.6 g of whole-rock sample powder, 0.4-0.6 g of pure olivine, or 0.08-0.09 g of pure chromite separate, 5 mL of double-purged, triple-distilled conc. HNO_3, 4 mL of triple-distilled conc. HCl, and appropriate amounts of mixed ^{185}Re-^{190}Os and HSE (^{99}Ru,^{105}Pd,^{191}Ir,^{194}Pt) spikes were sealed in double, internally-cleaned, chilled 25 mL Pyrex™

borosilicate Carius Tubes (CTs) and heated to 270°C for 96 h. Osmium was extracted from the acid solution by CCl_4 solvent extraction (Cohen and Waters, 1996), then back-extracted into HBr, followed by purification via microdistillation (Birck et al., 1997). Ruthenium, Pd, Re, Ir, and Pt were separated and purified using anion exchange chromatography (Rehkämper and Halliday, 1997). Average total analytical blanks during the analytical campaign were (in pg): Re 0.29±0.06, Os 0.21±0.06, Ir 0.38±0.17, Ru 1.5±0.8, Pt 14±9, and Pd 7±2 ($\pm 2\sigma_{mean}$, N = 9). For the whole-rock samples, the total analytical blanks for all HSE constitute less than 0.7% of the total element analyzed. For the olivine and chromite separates, the total analytical blanks for Os constitute less than 0.1%, and for Ir and Ru – less than 0.2% of the total element analyzed. Blank contributions for Re varied between 3% and 12%, for Pt – between 5% and 30%, and for Pd – between 3% and 70%.

Osmium isotopic measurements were accomplished via negative thermal ionization mass-spectrometry (NTIMS: Creaser et al., 1991). All samples were analyzed using a secondary electron multiplier (SEM) detector of a *ThermoElectron Triton* mass spectrometer at the *Isotope Geochemistry Laboratory (IGL),* University of Maryland. The measured isotopic ratios were corrected for mass fractionation using $^{192}Os/^{188}Os = 3.083$. The internal precision of measured $^{187}Os/^{188}Os$ in all samples was better than 0.05% ($2\sigma_{mean}$). The $^{187}Os/^{188}Os$ of 300 pg loads of the in-house Johnson-Matthey Os standard measured over the course of the entire analytical campaign averaged 0.11376±11 ($\pm 2\sigma_{stdev}$, N = 54). This value characterizes the external precision of the isotopic analysis (0.10%). We used this value to assess the true uncertainty on the measured $^{187}Os/^{188}Os$ ratio for each individual sample. The $^{187}Os/^{188}Os$ ratio measured in each sample was also corrected for the instrumental bias relative to the average $^{187}Os/^{188}Os = 0.11378$ measured in the Johnson-Matthey Os standard on the Faraday cups of the *IGL Triton*. The correction factor of 1.00018 was calculated by dividing this value by the average $^{187}Os/^{188}Os$ measured in the Johnson-Matthey Os standard on the SEM of this instrument.

The measurements of Ru, Pd, Re, Ir, and Pt were performed at the *IGL* via inductively coupled plasma mass-spectrometry (ICP-MS) using a *Nu Plasma* instrument with a triple electron multiplier configuration in a static mode. Isotopic mass fractionation was monitored and corrected for by interspersal of samples with standards. The accuracy of the data was assessed by comparing the results for the reference materials UB-N and GP-13 obtained during the ongoing analytical campaign. Concentrations of all HSE and Os isotopic compositions obtained at the *IGL* are in good agreement with the results from other laboratories (**Table 1**). Diluted spiked aliquots of iron meteorites were run during each analytical session as secondary standards. The results from these runs agreed within 1% for Re and Ir, and within 2% for Ru, Pt, and Pd, with fractionation-corrected values obtained from measurements of undiluted iron meteorite solutions using Faraday cups of the same instrument with signals of >100 mV for the minor isotopes. We therefore cite ±1% as uncertainty on the concentrations of Re and Ir, ±2% on the concentrations of Ru, Pt, and Pd, and ±0.1% on the concentrations of Os in the whole-rock samples. For the olivine and chromite separates, the uncertainties on the Os, Ir, and Ru abundances were the same as for the whole-rock samples, whereas the uncertainties on the Re concentrations were between 1.5% and 6%, Pt – between 2.5% and 15%, and Pd – between 1.5% and 35%, assuming a ~50% variation in abundances in the total analytical blank (TAB). The uncertainty on the Re concentration was the main source of uncertainty on the Re/Os ratio. For the

whole-rock samples, this uncertainty was, thus, estimated to be 1.0%, and for the olivine and chromite separates – between 1.5% and 6%.

All regression calculations were performed using ISOPLOT 3.00 (Ludwig, 2003). The uncertainties on the concentrations and isotopic ratios used for the regression calculations are as stated above. The initial $\gamma^{187}Os$ value was calculated as the per cent deviation of the isotopic composition at the time defined by the isochrons relative to the chondritic reference of Shirey and Walker (1998) at that time.

The average chondritic Os isotopic composition at the time defined by the isochrons was calculated using the ^{187}Re decay constant $\lambda = 1.666 \times 10^{-11}$ year^{-1}, an early Solar System initial $^{187}Os/^{188}Os = 0.09531$, and $^{187}Re/^{188}Os = 0.40186$ (Smoliar et al., 1996; Shirey and Walker, 1998).

3.2.2 Pt-Os isotopic data. In the present study, we followed the methodology developed by Puchtel et al. (2004a) and Puchtel et al. (2005) for determining precise initial $^{186}Os/^{188}Os$ and $^{187}Os/^{188}Os$ isotopic compositions in materials requiring corrections for the ingrowth of radiogenic ^{186}Os and ^{187}Os, such as Archean komatiites. This methodology involves high-precision simultaneous determination of $^{186}Os/^{188}Os$ and $^{187}Os/^{188}Os$ ratios on un-spiked digestions combined with determination of elemental abundance ratios of Pt, Re, and Os on small aliquots taken from the un-spiked digestions to ensure the representativeness of these ratios for each sample digestion. In order to obtain the amount of Os required for the high-precision measurements of the $^{186}Os/^{188}Os$ and $^{187}Os/^{188}Os$ ratios (~100 ng), each sample was digested in 4 to 20 CTs, depending on the Os concentrations in the sample. For the initial un-spiked digestions, ~3 g of sample powder, 9 mL of double-purged, triple-distilled conc. HNO_3, and 6 mL of triple-distilled conc. HCl were placed into a double, internally cleaned, 38 mL Pyrex™ CT chilled to 0°C, sealed and kept in an oven at 270°C for 96 hours. After the digestion was complete, the tubes were chilled and opened, 0.5 mL of the acid sample solution from each CT in the batch of 4 CTs representing a single sample digestion were transferred into a 25 mL Pyrex™ CT for precise determination of the Re/Os, Ir/Os (for monitoring potential Os losses during aliquot transfer), and Pt/Os ratios in each sample. Before the transfer procedure, the double, internally cleaned, 25 mL Pyrex™ CT was chilled to 0°C and appropriate amounts of the mixed ^{185}Re-^{190}Os and HSE spikes were added to it, followed by 4 mL of double-purged, triple-distilled conc. HNO_3 and 3 mL of triple-distilled conc. HCl, after the sample solution transfer was completed. The sealed CTs with the spiked sample solutions were kept in the oven at 270°C for 24 h to achieve sample-spike equilibration. After opening the CT, the spiked aliquots were processed using the same procedure utilized in the Re-Os and HSE analysis, except that, without a knowledge of the precise weight of the sample represented by the amount of the transferred solution, only the Re/Os, Pt/Os, and Ir/Os ratios were determined. From the remaining part of the un-spiked acid sample solutions, Os was extracted and purified using the same protocol utilized in the Re-Os study. The Os cuts from the batch of CTs, containing a single sample digestion, were combined into one cut and used for the precise measurements of the $^{186}Os/^{188}Os$ and $^{187}Os/^{188}Os$ ratios.

Measurements of Re, Os, Pt, and Ir isotopic compositions from the spiked aliquots, for the determination of precise Re/Os, Pt/Os, and Ir/Os ratios, were performed using the same protocol utilized in the Re-Os and HSE study outlined above.

The high-precision measurements of the $^{186}Os/^{188}Os$ and $^{187}Os/^{188}Os$ ratios were performed by *N-TIMS* in a static mode on a nine Faraday collector *ThermoFinnigan Triton*® mass spectrometer at the *IGL*. Signals of >100 mV on mass 234 ($^{186}Os^{16}O_3^-$) and 235 ($^{187}Os^{16}O_3^-$) were generated to reach the maximum in-run precisions for the $^{186}Os/^{188}Os$ and $^{187}Os/^{188}Os$ ratios. During each run, between 1400 and 2600 ratios were collected for each sample load, and the in-run uncertainties on the measured $^{186}Os/^{188}Os$ and $^{187}Os/^{188}Os$ ratios are quoted as $2\sigma_{mean}$. The possible isobaric interference of $^{186}W^{16}O_3^-$ on $^{186}Os^{16}O_3^-$ was assessed by measuring $^{184}Os/^{188}Os$ (modified if $^{184}W^{16}O_3^-$ present) and monitoring mass 231 ($^{183}W^{16}O_3^-$) using the electron multiplier. Although a signal of ~3-10 cps was normally measured at mass 231, its size in comparison to other potential isotopes of W indicated it was not W, and, therefore, no W corrections were made. Instead, the small signals typically observed at mass 231 are consistent with the expected amount of $^{198}Pt^{16}O^{17}O$ that is produced from the Pt filaments during ionization. This was indicated from the mass scan profiles from mass 226 ($^{194}Pt^{16}O_2$) to mass 230 ($^{198}Pt^{16}O_2$), that clearly show all of the PtO_2 isotopes in their expected proportions in the spectrum, and no evidence for WO_3 production at mass 230 or 231. The mean of the Johnson-Matthey Os standard runs during the period of data collection was 0.001306±5 for $^{184}Os/^{188}Os$, 0.1198454±16 for $^{186}Os/^{188}Os$, and 0.113788±13 for $^{187}Os/^{188}Os$ ($2\sigma_{stdev}$, N = 27). The uncertainty on the $^{186}Os/^{188}Os$ characterizes the external precision of the isotopic analysis (±14 ppm). We used this value to assess the true uncertainty on the measured $^{186}Os/^{188}Os$ ratio for each individual sample, and also to calculate the uncertainty on the average initial $^{186}Os/^{188}Os$ ratios. Since our high-precision $^{186}Os/^{188}Os$ ratios obtained at the *Johnson Space Center* and at *IGL* were previously bias-corrected to a common JM Os standard $^{186}Os/^{188}Os$ value of 0.1198475 (Puchtel et al., 2009b), the $^{186}Os/^{188}Os$ ratios measured in this study were also bias-corrected to $^{186}Os/^{188}Os$ = 0.1198475 using a correction coefficient of 1.0000177. To calculate the initial $^{186}Os/^{188}Os$ ratios, the Pt/Os ratios obtained from the spiked runs and the ^{190}Pt decay constant $\lambda = 1.477 \times 10^{-12}$ year^{-1} (Begemann et al., 2001) were used. The initial $\varepsilon^{186}Os$ values were calculated as part per 10,000 deviation of the $^{186}Os/^{188}Os$ ratio in the sample at the time of lava emplacement relative to the chondritic reference of Brandon et al. (2006) at that time using an early Solar System initial $^{186}Os/^{188}Os$ = 0.1198269 at T = 4567 Ma and $^{190}Pt/^{188}Os$ = 0.00174.

4. Results

4.1. Re-Os isotopic data

The Re-Os isotopic data for the whole-rock samples and olivine and chromite separates from the Komati and Weltevreden komatiite systems are presented in **Table 2** and plotted on Re-Os isochron diagrams in **Fig. 1**.

For the Komati system, the data for 15 whole-rock samples, including two replicates and three averages for the spiked aliquots of the unspiked digestions processed for the Pt-Os study to

331 determine the Re/Os and Pt/Os ratios (marked with (*) in **Table 2**), and four pure olivine and
332 chromite separates, define an errochron (MSWD = 4.7) with a slope corresponding to an age of
333 3484±38 Ma and an initial $^{187}Os/^{188}Os$ = 0.10335±15 ($\gamma^{187}Os$ = +0.34±0.15, $2\sigma_{mean}$). Sample
334 BV14, a cumulate from the bottom of flow 11 (see Fig. 1 in Puchtel et al., 2013), which is among
335 the most altered samples, plots to the right of the regression line. Its high Re/Os is only partially
336 supported by the respective ingrowth of ^{187}Os and, as such, is likely due to the late addition of
337 Re. This sample was excluded from the isochron regression calculations.
338 For the Weltevreden system, the data from this study, including four averages of the spiked
339 aliquots of the unspiked digestions (also marked with (*) in **Table 2**), combined with those
340 reported by Connolly et al. (2011), define a precise isochron (MSWD = 0.7) with an age of
341 3263±12 Ma and an initial $^{187}Os/^{188}Os$ = 0.10442±4 ($\gamma^{187}Os$ = -0.14±0.04, $2\sigma_{mean}$). This age and
342 the $^{187}Os/^{188}Os$ initial ratio, albeit derived from a much larger dataset, are identical to those
343 reported by Connolly et al. (2011). Sample SA501-7, collected from the B_1 subzone of flow
344 SA501 (see Fig. 2 in Puchtel et al., 2013), plots to the right of the regression line. For reasons
345 discussed in Connolly et al. (2011), this sample was excluded from the isochron regression
346 calculations.
347
348 ***4.2. Pt-Os isotopic data***
349 The Pt-Os isotopic data for the Komati and Weltevreden komatiite systems are presented in
350 **Table 3** and are plotted on Pt-Os isochron diagrams in **Fig. 2**. The three samples analyzed,
351 including one replicate, from the Komati Fm. plot with a very limited spread in the Pt/Os ratios
352 below the 3484 Ma chondritic reference line. The average initial $^{186}Os/^{188}Os$ ratio, calculated for

353 the emplacement age of 3484 Ma and using the measured $^{190}Pt/^{188}Os$ and $^{186}Os/^{188}Os$ ratios in the
354 individual samples, is 0.1198283±9 (initial $\varepsilon^{186}Os$ = -0.12±0.08, $2\sigma_{mean}$).
355 The four samples analyzed, including one replicate, from the Weltevreden Fm., are also
356 characterized by a limited spread in the Pt/Os ratios, but, unlike the Komati system samples, plot
357 well above the 3263 Ma chondritic reference line. The average initial $^{186}Os/^{188}Os$ ratio,
358 calculated for the emplacement age of 3263 Ma using the measured $^{190}Pt/^{188}Os$ and $^{186}Os/^{188}Os$
359 ratios in the individual samples, is 0.1198330±8 (initial $\varepsilon^{186}Os$ = +0.22±0.07, $2\sigma_{mean}$). The
360 uncertainties on both initial ratios are calculated by dividing the long-term external
361 reproducibility for the $^{186}Os/^{188}Os$ ratio in the in-house Johnson-Matthey Os standard obtained
362 during the analytical campaign (±14 ppm) by the square root of the number of samples analyzed
363 for each komatiite system.
364
365 ***4.3. HSE abundance data and compositions of the emplaced komatiite lavas***
366 The abundances of the HSE in the Komati and Weltevreden whole-rock komatiite samples
367 and olivine and chromite separates are presented in **Table 4** and plotted on MgO variation
368 diagrams in **Fig. 3**; the CI chondrite-normalized abundances (using average values for the
369 chondrite Orgueil from Horan et al., 2003) are plotted in **Figs. 4 and 5**.
370 The olivine and chromite separates from the Komati system exhibit similar CI chondrite-
371 normalized patterns with chondritic to slightly sub-chondritic Os/Ir, and enrichments in Os, Ir,
372 and especially Ru, relative to Pt and Pd. The chromite has about two orders of magnitude higher
373 Os, Ir, and Ru, and about an order of magnitude higher Pt and Pd contents, compared to the
374 olivine. These patterns and abundances are generally consistent with experimental studies of

HSE partitioning between olivine, chromite and silicate melt (Brenan et al., 2003; Brenan et al., 2005; Brenan et al., 2012).

The olivine separates from the Weltevreden system exhibit slightly supra-chondritic Os/Ir ratios and are characterized by about one order of magnitude higher Os and Ir, and a factor of two higher Ru contents, compared to the Komati olivines. This pattern of elevated Os and Ir relative to Ru contents is not consistent with effects predicted for magmatic partitioning behavior of these elements between olivine and silicate melt (Brenan et al., 2003; Brenan et al., 2005), and may indicate the presence of sub-micron-sized inclusions of Os-Ir alloys in the Weltevreden olivine separates.

The variations in the Pt and Pd abundances *versus* MgO contents in the whole-rock samples are consistent with the typical incompatible behavior of Pt and Pd during komatiite lava differentiation. The Pt and Pd data for both komatiite systems follow tight trends with negative slopes that pass through the measured respective olivine compositions, indicating that olivine was the only liquidus phase that controlled the concentrations of these elements during differentiation of the Komati and Weltevreden lavas, and, at the same time, providing evidence for the immobile behavior of Pt and Pd during seafloor alteration and metamorphism (**Fig. 3**).

The Re data for the whole-rock samples from the Komati system show a great deal of scatter on the Re vs. MgO diagram (**Fig. 3**). As mentioned earlier, sample BV14, which has the highest Re content of all, is the one sample that plots beyond analytical uncertainties off the Re-Os isochron (**Fig. 1**), presumably due to post-emplacement Re enrichment. The rest of the samples, however, plot on the isochron that is consistent with the emplacement age of the lavas. This indicates that the post-magmatic processes that acted on these lavas, e.g., seafloor alteration,

were nearly contemporaneous with the lava emplacement, and that the Re-Os system remained closed since then.

The Re data for the whole-rock samples from the Weltevreden system, with two exceptions, plot on the well constrained regression line that passes through the measured olivine compositions (**Fig. 3**); one of the exceptions also plots off the Re-Os isochron (**Fig. 1**). Based on this observation, we conclude, also following Connolly et al. (2011), that Re in the Weltevreden system, with the exception of the two samples, displays magmatic behavior and was essentially immobile during seafloor alteration and metamorphism.

Among the HSE we analyzed, Re is the most fluid-mobile element; Pd and especially Pt are much less mobile (e.g., Colodner et al., 1992; Puchtel et al., 2007), and Os, Ir, and Ru are even less mobile than Pt. This observation allows us to extend the conclusion regarding the immobility of Pt and Pd, to Os, Ir, and Ru, for both komatiite systems.

Variations of the Os and Ir abundances in the Komati and Weltevreden systems show similar patterns, although the magnitude of the variations is a factor of three larger in the latter (**Figs. 3 and 4**). The upper chilled margin samples from both systems contain ~1.4 ppb Os (and Ir). The spinifex zones show a typical pattern of decreasing Os and Ir abundances with decreasing the MgO contents. The largest range of variations in both systems (e.g., the Os abundances vary between 1.0 and 3.7 ppb in the Komati and between 1.0 and 12.0 ppb in the Weltevereden systems) is observed among olivine cumulate samples with essentially identical MgO contents. Furthermore, there is a general decrease in Os and Ir contents in the upper parts, and an increase in the lower parts of the olivine cumulate zones, relative to those in the chilled margin samples. The olivine separates, on the other hand, are characterized by highly variable Os and Ir contents that are either lower (Komati) or higher (Weltevereden) than those in the chilled margin samples.

These observations indicate that the Os and Ir abundances in the cumulate portions of the Komati and Weltevreden komatiite lava flows were not controlled by fractionation of olivine, but rather by an Os-Ir rich phase, such as an Os-Ir alloy. This interpretation was previously put forward for so-called Munro-type komatiitic lavas (Puchtel and Humayun, 2005), i.e., the komatiitic lava flows that exhibit positive correlations between Os, Ir abundances and the MgO contents, as opposed to the Kostomuksha-type lavas, which exhibit negative correlations. The observed pattern of Os and Ir depletions in the upper parts of cumulate zones and enrichments in the lower parts relative to the compositions of the chilled margin samples has been previously documented for some Abitibi komatiite lavas (Puchtel et al., 2004b). This observation lends further support to the notion that olivine does not play a major role in controlling Os and Ir abundances during komatiite lava differentiation (Puchtel and Humayun, 2001; Puchtel et al., 2004b; Barnes and Fiorentini, 2008), and is consistent with the experimental data of Brenan et al. (2005).

Ruthenium abundances show minimal variations across the lava flows from both komatiite systems **(Fig. 3)**, indicating that the bulk solid-liquid partition coefficient for Ru was close to unity, consistent with trends also established for late Archean komatiite systems (e.g., Puchtel et al., 2004b; Puchtel and Humayun, 2005; Puchtel et al., 2007; Barnes and Fiorentini, 2008). With a few exceptions, samples plot on olivine control lines in Ru *vs*. MgO diagrams (**Fig. 3**), consistent with the notion that variations of Ru abundances in komatiite lavas were controlled largely by fractionation of olivine (Brenan et al., 2003; Barnes and Fiorentini, 2008). Several cumulate samples plot above the olivine control lines (**Fig. 3**). These samples also have somewhat elevated Cr concentrations (Puchtel et al., 2013), which may indicate the presence of small amounts of cumulus chromite with associated platinum-group minerals, as suggested previously (Puchtel and Humayun, 2001; Barnes and Fiorentini, 2008; Brenan et al., 2012).

In order to calculate the HSE abundances in the emplaced komatiite lavas, we used the ISOPLOT (Ludwig, 2003) bivariate linear regression analysis, assuming the MgO contents in the emplaced lavas of 29.4±0.4 and 31.4±0.9% for the Komati and Weltevreden systems, respectively (Puchtel et al., 2013); the results are presented in **Table 5**. The projected emplaced lava for the Komati system contained (ppb) 1.3±0.1 Os, 1.4±0.1 Ir, 3.6±0.2 Ru, 4.8±0.4 Pt, and 4.7±0.4 Pd, as compared to 1.4±0.1 Os, 1.5±0.1 Ir, 6.3±0.2 Ru, 8.5±0.5 Pt, and 6.6±0.5 Pd for the Weltevreden system. The Re content in the Weltevreden emplaced lava is calculated to be 0.33±0.03 ppb, whereas Re content in the Komati emplaced lava cannot be calculated due to post-eruption mobility of Re. The emplaced lavas from the Komati and Weltevreden systems, thus, had chondritic to slightly sub-chondritic CI-normalized Os/Ir_N = 0.93±0.05 and 0.94±0.08, respectively, and similarly moderately fractionated HSE patterns (Pd/Ir_N = 2.7±0.2 and 3.5±0.2, respectively). The absolute Ru and Pd abundances are ~50% higher and Pt abundances were about a factor of two higher in the emplaced Weltevreden lava compared to its Komati counterpart (**Fig. 4**). This indicates significant Pt enrichment, compared to the HSE with similar compatibility, such as Pd, in the Weltevreden system.

5. Discussion

5.1. Absolute and relative HSE abundances in the sources of the Komati and Weltevreden komatiite systems

The Re-Os and Pt-Os isotopic systems are partially or wholly governed by the strong partitioning of these elements into metal or sulfide liquid, relative to silicate melt. Additionally, during mantle melting, Os is typically compatible with the melting residue, whereas Pt and Re are incompatible (Barnes et al., 1985; Rehkämper et al., 1999b). The Re-Os and Pt-Os isotopic

systems, therefore, provide valuable insights into certain processes, to which the more traditional, lithophile element-based isotopic systems, are less sensitive. These processes include planetary accretion and mantle/core differentiation.

The initial $^{186}Os/^{188}Os$ and $^{187}Os/^{188}Os$ ratios obtained in the Pt-Os and Re-Os isotopic studies of a range of mantle-derived materials provide measures of long-term evolution of Pt/Os and Re/Os in the mantle. These studies to-date have produced a remarkably variable array of data that has been used to constrain Re-Os and Pt-Os isotopic parameters of major mantle reservoirs (see review in Walker (2009) and references therein), such as the putative Primitive Mantle (PM) and Depleted MORB Mantle (DMM). The evolution trajectories for current estimates of these major reservoirs are plotted in **Fig. 6** and are further used as reference parameters.

The modern Os isotopic composition of the PM, i.e., hypothetical mantle reservoir that has not experienced melt depletion, has been constrained on the basis of studies of global suites of mantle xenoliths ($\gamma^{187}Os = +2.04\pm0.63$: Meisel et al., 2001), as well as Os-rich alloys ($\varepsilon^{186}Os = +0.10\pm0.13$: Walker et al., 2005; Brandon et al., 2006).

The Os isotopic composition of the DMM, or modern convecting upper mantle that has lost melt due to extraction of oceanic crust, is a controversial issue, with as much as a ~3% difference in average $^{187}Os/^{188}Os$ obtained from abyssal peridotites (Snow and Reisberg, 1995; Brandon et al., 2000; Liu et al., 2009) compared with estimates based on projections to the present from Proterozoic and Phanerozoic ophiolites (Walker et al., 1996; Tsuru et al., 2000; Walker et al., 2002). The $\gamma^{187}Os$ value of the DMM, based on data compiled for abyssal peridotites, is -1.40 ±0.93 (Snow and Reisberg, 1995; Brandon et al., 2000; Liu et al., 2009). In comparison, the $\varepsilon^{186}Os$ value of DMM, based on a still limited data for abyssal peridotites (Brandon et al., 2000), is -0.27 ± 0.07 ($2\sigma_{mean}$).

Here, we use the initial $^{186}Os/^{188}Os$ and $^{187}Os/^{188}Os$ ratios obtained for the Komati and Weltevreden systems as a measure of long-term evolution of Pt/Os and Re/Os in the early Archean mantle sources of these komatiite systems. In order to constrain the long-term source characteristics, we calculate the parent/daughter elemental ratios necessary to achieve isotopic compositions at the times of komatiite formation by initially assuming formation of the mantle domains at the time of Solar System formation. It is calculated that the Komati source would have evolved from early Solar System initial ratios for $^{186}Os/^{188}Os = 0.1198269$ at 4.567 Ga (Brandon et al., 2006) and $^{187}Os/^{188}Os = 0.09531$ at 4.558 Ga (Shirey and Walker, 1998), to the komatiite initial $^{186}Os/^{188}Os = 0.1198283\pm9$ and $^{187}Os/^{188}Os = 0.10334\pm8$ at 3484 Ma, with time-integrated $^{190}Pt/^{188}Os = 0.00085\pm56$ and $^{187}Re/^{188}Os = 0.419\pm4$. The Weltevreden source would have evolved to its initial $^{186}Os/^{188}Os = 0.1198330\pm8$ and $^{187}Os/^{188}Os = 0.10442\pm4$ at 3263 Ma with time-integrated $^{190}Pt/^{188}Os = 0.00312\pm41$ and $^{187}Re/^{188}Os = 0.396\pm2$. Although the time-integrated $^{187}Re/^{188}Os$ in both sources are similar to the chondritic reference value of 0.402 (Shirey and Walker, 1998), the $^{190}Pt/^{188}Os$ are non-chondritic. For the Komati system, the $^{190}Pt/^{188}Os$ is subchondritic. When the full uncertainty on the calculated $^{190}Pt/^{188}Os$ in the Komati system is considered (±0.00056), the highest value permitted by the uncertainty (0.00141) is still ~12% lower than the lowest $^{190}Pt/^{188}Os$ recorded in any group of chondrites (the average values are 0.00177±20, 0.00175±16, and 0.00178±11 ($2\sigma_{stdev}$) in carbonaceous, ordinary, and enstatite chondrites, respectively, as compiled from data of Horan et al. (2003) and Brandon et al. (2005a)).

For the Weltevreden system, the calculated $^{190}Pt/^{188}Os$ of its source is suprachondritic. When the full uncertainty on the calculated $^{190}Pt/^{188}Os$ in the Weltevreden source is considered (±0.00041), the lowest value permitted by the uncertainty (0.00271) is 40% higher than the

highest $^{190}Pt/^{188}Os$ recorded in any group of chondrites. In reality, the reservoirs that the Komati and Weltevreden system komatiites were derived from likely formed sometime after Solar System formation, so the requisite Pt/Os ratios in the sources of both systems would have to have been even more fractionated from the chondritic reference. This will be discussed in the following sections.

It is well established that in the mantle, the platinum-group elements (PGE) are largely hosted by sulfides and/or by PGE alloys (Barnes et al., 1985; Lorand et al., 1999; Rehkämper et al., 1999b; Lorand and Alard, 2001; Luguet et al., 2007), whereas Re resides in both silicates and sulfides (Reisberg and Lorand, 1995; Fonseca et al., 2007; Brenan, 2008). There are two principal types of sulfides in the mantle – high-temperature monosulfide solid solution, Mss, that usually occurs as inclusions in silicates, mostly in olivine, and the lower-temperature Cu-Ni-rich sulfides, that are usually interstitial to major silicate minerals (Luguet et al., 2007). The Mss preferentially accommodates Os, Ir, and Ru, whereas the Cu-Ni-rich sulfides preferentially host Pt, Pd, and Re. Osmium-Ir-Ru alloys are usually residual phases remaining and/or forming in refractory mantle peridotites (e.g., harzburgites) in response to consumption of sulfides during high-degrees (>25%) partial melting (Keays, 1995; Luguet et al., 2007).

In order to calculate the absolute abundances of the HSE in the sources of the Komati and Weltevreden komatiite systems, we use the technique that has been previously developed and applied in studies of other komatiite systems (e.g., Puchtel et al., 2004b; Puchtel and Humayun, 2005). This technique is based on the assumption that an element behaves similarly during both partial melting in the mantle source and fractional crystallization of the erupted lava. Thus, if an HSE was incompatible with the liquidus mineral assemblage during differentiation of an emplaced komatiite lava, it was also likely similarly incompatible with the residual mineral

assemblage during melting that produced the lava. For a specific komatiite lava suite, the abundances of elements that are incompatible with the melting residue (i.e., the mineral hosts of these elements have been exhausted during melting) should plot on the liquid lines of descent. The latter can be established via regressing the abundances of the incompatible elements vs. MgO contents in the lavas. The source concentrations of the incompatible elements can then be calculated via projecting the abundances in the lavas to the assumed MgO content in the source (the so-called projection technique). Since the MgO content of the mantle is little affected by variations in the degree of previous melt extractions, Puchtel et al. (2004b) used the average MgO content of 38% for depleted spinel peridotites sampled worldwide, which is also the accepted value for the putative PM (McDonough and Sun, 1995).

It should be noted, however, that the sulfur content at saturation of a mafic magma increases with decreasing pressure, so magmas may become undersaturated during adiabatic ascent (Mavrogenes and O'Neill, 1999). As a result, the bulk HSE partition coefficients of the first phases to fractionate could differ from those that last enter the melt during partial melting. This limitation can only be relaxed if there are no sulfides left in the source after melt separates from the residue. Therefore, one of prerequisites for this methodology to be applicable for calculating the HSE composition of a mantle source of lavas from their HSE abundances is the complete exhaustion of low-temperature Cu-Ni-rich sulfides in the source during partial melting. This can only be attained if the degree of melting exceeds ~30% (Barnes et al., 1985; Keays, 1995; Rehkämper et al., 1999b); this degree of melting is typical of komatiite formation.

The assumption of complete exhaustion of Cu-Ni-rich sulfides in the sources can be tested against the behavior of PGE that are largely controlled by these sulfides during melting and differentiation. Compatible behavior of Pt and Pd, as well as chalcophile elements, such as Cu,

Zn, and Ga, during lava differentiation is normally associated with sulfide-saturated conditions, such as those that obtained during formation of lower degree melts, e.g., MORB (Hamlyn et al., 1985; Peach et al., 1990; Bezos et al., 2005). By contrast, the observation that Pt and Pd, as well as chalcophile elements Ga and Zn (Puchtel et al., 2013), behaved strongly incompatibly during differentiation of both Komati and Weltevreden lavas (**Fig. 3**), provides strong evidence that these two komatiite systems were sulfide-undersaturated upon lava emplacement. This is an important observation that also indicates that both the Komati and Weltevreden komatiite magmas did not undergo sulfide liquid fractionation prior to emplacement, and, thus, their HSE inventories were likely preserved *en route* from mantle source to surface eruption.

In order to estimate the abundances of the incompatible HSE (Re, Pt, and Pd) in the Komati and Weltevreden sources, we project the abundances of these elements measured in the lavas and in the olivine separates for each of the two komatiite systems to MgO = 38 wt%. The resulting projected source abundances are presented in **Table 5**. The concentrations of Pt calculated by means of ISOPLOT-regression of data for both whole-rock samples and olivine separates, are 2.9±0.2 ppb and 6.0±0.4 ppb, and for Pd are 2.9±0.2 ppb and 4.6±0.3 ppb ($2\sigma_{mean}$) in the Komati and Weltevreden sources, respectively. The Re abundance in the source of the Weltevreden system is calculated to be 0.23±0.02 ppb ($2\sigma_{mean}$). Due to evidence for post-eruption mobility of Re in the Komati lavas, its abundance in the Komati source cannot be calculated directly using this technique, but is estimated using the Os isotopic data, below.

To calculate the Ru abundances in the sources, we used the observation that olivine fractionation was the main control on the variations of Ru abundances in both systems. As such, we used the linear regressions of Ru vs. MgO in **Fig. 3** to obtain Ru abundances in the sources of the Komati and Weltevreden systems to be 3.5±0.3 ppb and 6.0±0.3 ppb, respectively.

The observed compatible behavior of Os and Ir during lava differentiation indicates that the emplaced lavas were saturated with respect to the hosts of these elements. As such, concentrations of Os and Ir in the sources of the Weltevreden and Komati lavas cannot be calculated directly using the projection technique. The Os contents must be estimated indirectly using the calculated Pt (for the Komati system) and Re (for the Weltevreden system) abundances in their sources, and the time-integrated $^{190}Pt/^{188}Os$ and $^{187}Re/^{188}Os$ derived from the initial $^{186}Os/^{188}Os$ and $^{187}Os/^{188}Os$ for the Komati and Weltevreden systems, respectively, using the following equations:

$$Os = Pt/(1047\times{}^{190}Pt/^{188}Os),\ Os = Re/(0.2115\times{}^{187}Re/^{188}Os) \quad (1)$$

$$^{190}Pt/^{188}Os = (^{186}Os/^{188}Os_i - 0.1198269)/(\exp(\lambda_1\times 4.567) - \exp(\lambda_1\times T)) \quad (2)$$

$$^{187}Re/^{188}Os = (^{187}Os/^{188}Os_i - 0.09531)/(\exp(\lambda_2\times 4.558) - \exp(\lambda_2\times T)) \quad (3)$$

where *i* denotes the respective Os initial isotopic ratio calculated for the time of the lava emplacement *T*, and λ_1 and λ_2 are decay constants of ^{190}Pt and ^{187}Re, respectively. The uncertainties on the Os concentrations are derived from the uncertainties on the initial Os isotopic compositions and on the calculated Pt and Re concentrations. The uncertainties on the Os abundances derived from (2) are relatively large compared to those calculated from (3).

The calculated time-integrated Os concentrations are 3.3±1.1 ppb and 2.7±0.2 ppb for the Komati and Weltevreden systems, respectively. The time-integrated Re content in the Komati source is then calculated to be 0.29±0.10 ppb. The Ir abundances in the sources are calculated using the Os contents and the Os/Ir in the emplaced komatiite lavas on the basis of the observation that during high-degree partial melting, komatiite melts mimic the Os/Ir ratios of

604 their mantle sources due to complete exhaustion of low-temperature Cu-Ni sulfides and Os-Ir
605 alloy saturation in the former (Fonseca et al., 2011; Fonseca et al., 2012). The calculated Ir
606 contents are 3.5±1.2 ppb and 3.0±0.3 ppb in the Komati and Weltevreden komatiite systems,
607 respectively.
608
609 ***5.2. The origin of the absolute and relative HSE abundances in the sources of the Komati***
610 ***and Weltevreden komatiite systems***
611 As is evident from **Fig. 6**, the sources of Archean komatiite systems, as well as 3.81 Ga
612 peridotites from Isua (Bennett et al., 2002), are characterized by initial $^{187}Os/^{188}Os$ that are
613 identical, within the uncertainty, to the chondritic reference of Shirey and Walker (1998), with
614 initial $\gamma^{187}Os$ values ranging, with two exceptions (the 2.8 Ga Kostomuksha and 3.55 Ga
615 Schapenburg systems), only from -0.1 to +0.4 (**Fig. 6**). These nearly uniform initial ratios are
616 difficult to place in the context of the evolution trajectories for contemporary mantle reservoirs
617 presented in **Fig. 6**, as the initial Os isotopic compositions of the komatiite sources lie largely
618 below the $\gamma^{187}Os$ evolution trajectory of the putative PM, yet well above the evolution trajectory
619 for the contemporary DMM, as based on abyssal peridotites. One explanation might be that these
620 komatiite systems were derived from lower mantle sources, with Os isotopic evolution different
621 from that of the oceanic mantle, as would be expected if they were generated within plumes
622 rising from the lower mantle. Consistent with this, there is strong petrologic/geochemical
623 evidence for a plume origin for both the Komati and Weltevreden komatiites (Puchtel et al.,
624 2013), as well as for most other komatiite systems presented in **Fig. 6** (Campbell et al., 1989;
625 Puchtel et al., 1997; Puchtel et al., 1998; Puchtel et al., 1999; Puchtel et al., 2009a; Puchtel et al.,
626 2009b). As such, the sources of these komatiites may have had distinct, lower mantle HSE

627 characteristics, as was also proposed by studies that involved a combination of ^{182}W – $^{186,187}Os$
628 (Touboul et al., 2012) and $^{142,143}Nd$ – Lu-Hf (Puchtel et al., 2013) isotopic systems.
629 The limited dataset of initial $^{186}Os/^{188}Os$ ratios that has been generated for komatiite systems
630 indicate that mantle sources of two late Archean systems, Abitibi and Belingwe (Puchtel et al.,
631 2004a; Puchtel et al., 2009b) evolved with time-integrated Pt/Os within the chondritic range. The
632 high initial $^{186}Os/^{188}Os$ and $^{187}Os/^{188}Os$ of the mantle source of the 2.8 Ga Kostomuksha
633 komatiites, however, requires an enriched, long-term suprachondritic Pt/Os and Re/Os (Puchtel
634 et al., 2005).
635 Of the two early Archean komatiite systems examined here, the Komati system evolved with
636 time-integrated Pt/Os that was below the chondritic value. By contrast, the Weltevreden source
637 evidently evolved with a strongly supra-chondritic Pt/Os ratio. Despite the difference in initial
638 $^{186}Os/^{188}Os$, the time-integrated Re/Os for both komatiite systems are well within the range of
639 those in chondrites.
640 Next, we consider the types of processes that could have caused such types of fractionations.
641 These cannot be either core-mantle interaction (Walker et al., 1995; Walker et al., 1997; Brandon
642 et al., 1998; Brandon and Walker, 2005; Humayun, 2011) or oceanic lithosphere recycling
643 (Walker et al., 1991; Lassiter and Hauri, 1998), as both processes should result in long-term
644 coupled enrichments in Re/Os and Pt/Os, albeit to a different relative degree.
645 The long-term fractionations of Pt/Os observed in the sources of the Komati and
646 Weltevreden komatiite systems must have occurred very early in Earth history, as required by
647 the ages of the komatiites, coupled with the length of time required to grow the observed
648 $^{186}Os/^{188}Os$ isotopic anomalies. Recently, based on the results of lithophile trace element and
649 $^{142,143}Nd$ and Lu-Hf isotope studies, (Puchtel et al., 2013) argued that both the Komati and

650 Weltevreden komatiites were derived from mantle domains that formed as late as 4400 Ma, as a
651 result of crystallization of a primordial magma ocean, with Mg-perovskite and minor Ca-
652 perovskite acting as fractionating mineral phases. The Pt/Os fractionation inferred for the source
653 of the Weltevreden komatiite system, as well as the less pronounced fractionation likely required
654 for the Komati source, could also be the result of such primordial differentiation, although the
655 mechanisms involved, due to the contrasting behaviors of the lithophile and highly siderophile
656 parent and daughter elements during planetary differentiation, must be different.
657 Recently, on the basis of combined ^{182}W and ^{186,187}Os isotopic data, Touboul et al. (2012)
658 argued that the mantle source of the 2.8 Ga Kostomuksha komatiite system included material
659 from a primordial reservoir that represented either a deep mantle region that underwent metal-
660 silicate equilibration, or a product of large-scale magmatic differentiation of the mantle. The
661 short-lived nature of the ^{182}Hf-^{182}W system ($t_{½}$ ~9 Ma) requires that the isotopically anomalous
662 reservoir formed within the first 30 million years of Solar System history. These authors also
663 concluded that the preservation of this reservoir, until at least 2.8 billion years ago, is strong
664 evidence for sluggish mixing of at least some portions of the mantle throughout the Hadean and
665 Archean. The mantle domains that preserved the ^{143}Nd and ^{176}Hf memory of an early mantle
666 differentiation event and ultimately gave rise to the Komati and Weltevreden komatiite sources
667 (Puchtel et al., 2013), may also have preserved the Re-Os and Pt-Os memory of this event. The
668 question that remains, then, is the nature of the mechanism that was responsible for the
669 fractionation of the Pt/Os in the sources of these komatiites, but did not detectably affect the
670 Re/Os. The process that holds the key to the lithophile element differentiation may provide some
671 clues to the HSE differentiation as well.

672 It has been shown by several authors that Mg-perovskite, the dominant lower mantle mineral,
673 has a strong affinity for Fe_2O_3; the latter is so strong that its Fe^{3+} content is independent of
674 oxygen fugacity (Frost et al., 2004; Wade and Wood, 2005; Frost et al., 2008). High levels of
675 Fe^{3+} are present in perovskite, even when it is in chemical equilibrium with metallic iron. Since
676 the lower mantle must have been poor in Fe_2O_3 during core formation, FeO would have
677 disproportionated to produce Fe_2O_3 to form Mg-perovskite and iron metal. Frost et al. (2004) and
678 Frost and McCammon (2008) argue that, following crystallization of a putative magma ocean,
679 the lower mantle must have contained approximately 1 wt% of a metallic iron-rich alloy. The
680 fate of this iron alloy is not clear. Wade and Wood (2005) and Frost et al. (2008) suggest that the
681 loss of some of this iron metal to the core is required to bring the oxidation state of the mantle to
682 its present levels. The dispersal of the residual iron metal in the lower mantle, as might have
683 occurred via magma ocean crystallization and/or overturn, might also have facilitated the
684 fractionation of Pt from other HSE in some lower mantle domains.
685 Experimental data indicate that, under the reducing conditions expected during crystallization
686 of a primordial magma ocean (Frost et al., 2008), Pt has strong tendency to form Fe-Pt alloys
687 (Borisov and Palme, 1997, , 2000). This tendency is much less for Pd and essentially does not
688 occur for the other HSE. Some portion of the iron metal that formed as a result of
689 disproportionation of FeO during crystallization of Mg-perovskite at the bottom of a magma
690 ocean might have combined with Pt to form Fe-Pt alloys. Dispersal of Fe-Pt alloys to lower
691 mantle domains could have resulted in the creation of Pt-enriched and Pt-depleted domains. The
692 enrichments and depletions would not necessarily correlate with enrichments and depletions in
693 the other HSE, so high- and low Pt/Os domains may have been created. Such a scenario can
694 potentially explain the observed time-integrated non-chondritic Pt/Os, coupled with the

chondritic Re/Os, in the sources of the Komati and Weltevreden komatiite systems. This fractionation must have occurred simultaneously with the major silicate differentiation established on the basis of the ^{142,143}Nd-^{176}Hf isotopic study (Puchtel et al., 2013), i.e., as late as 4400 Ma, and the mantle reservoirs sampled by the Weltevreden lavas must have remained isolated from the rest of the mantle not only in terms of the lithophile element (Puchtel et al., 2013), but also in terms of the Re-Pt-Os isotope systematics.

Assuming that our conclusions about the nature of the Pt/Os fractionation in the sources of the Komati and Weltevreden systems are correct, we can calculate the original Pt abundances that existed in the sources of both systems prior to the 4400 Ma differentiation event. Since both sources are characterized by chondritic initial ^{187}Os/^{188}Os, and, thus, evolved with time-integrated chondritic ^{187}Re/^{188}Os ratios, it is logical to assume that their initial ^{186}Os/^{188}Os ratios prior to the major silicate differentiation event (4400 Ma) were also chondritic, and, thus, these systems evolved up to that point in time with chondritic ^{190}Pt/^{188}Os. As such, we solve equations (1-3) for Pt, using the Os concentrations calculated from the Pt-Os (Komati: 3.3±1.1 ppb Os) and Re-Os (Weltevreden: 2.7±0.2 ppb Os) isotopic data and assuming chondritic evolution to 4400 Ma. Our calculations yield the Pt abundances of 5.9±0.9 ppb and 4.9±0.7 ppb in the sources of the Komati and Weltevreden komatiite systems, respectively, with the uncertainties defined by both the uncertainties on the initial ^{186}Os/^{188}Os isotopic compositions and on the calculated Os abundances.

The HSE concentrations in the Komati and Weltevreden komatiite sources, calculated using the assumptions discussed above (**Table 5),** are plotted as CI chondrite-normalized abundances in **Fig. 7**, together with an estimate of average HSE abundances in the sources of late Archean komatiite systems compiled on the basis of data of Puchtel et al. (2004a; 2004b; 2007, 2009b)

718 and Puchtel and Humayun (2005). These data are compared with the HSE abundances estimated
719 for the modern PM of Becker et al. (2006).

720 The CI chondrite-normalized abundances in the sources of the two komatiite systems display
721 contrasting, differently fractionated patterns. The Komati system source is depleted in Pt and Pd
722 relative to Os and Ir (Pd/Ir_N = 0.83±0.29), whereas the Weltevreden system source is enriched in
723 Pt and Pd over Os and Ir (Pd/Ir_N = 1.6±0.1). Interestingly, the combined Komati-Weltevreden
724 komatiite system source, calculated as an average of the HSE abundances present in the two
725 sources, exhibit near-chondritic CI chondrite-normalized HSE patterns, with Pd/Ir_N = 1.2.

726 In **Fig. 8**, the calculated absolute abundances of HSE in the sources of the Komati and
727 Weltevreden komatiite systems are plotted as a function of age and are compared with the HSE
728 abundances in the sources of late Archean komatiite systems and in the estimate of the modern
729 PM. Since, out of all HSE, Pt and Pd (and Re, where post-emplacement mobility was not an
730 issue) are determined with the highest degree of confidence for all komatiite systems, only the
731 total concentrations of Pt and Pd are plotted and compared. In the calculations of the totals, the
732 relative weight of the Pd contribution to the total was normalized to that of Pt on the basis of
733 their relative abundances in an average CI chondrite Orgueil (Horan et al., 2003) using 1.52 as a
734 normalizing coefficient.

735 The first observation evident from **Fig. 8** is that the total Pt+Pd abundances in the sources of
736 the near-contemporaneous late Archean komatiite systems span a substantial range, from as little
737 as 58±7% in the 2.69 Ga Belingwe system to as much 85±5% in the 2.72 Ga Abitibi system, of
738 the total Pt and Pd present in the estimates for the modern PM. The uncertainty on the total Pt
739 and Pd abundances in the latter are such that the total Pt and Pd abundances in some late Archean
740 komatiite systems, e.g., Abitibi and Kostomuksha, overlap with those in the estimates for the

PM, whereas others (Vetreny, Belingwe, Volotsk-Kenozero) do not. The second observation is that the total Pt and Pd abundances in the sources of the early Archean komatiite systems are within the range of those in the late Archean komatiite systems, albeit on the lower side, varying from 56±12% for the Komati to 65±10% for the Weltevreden, of the total Pt and Pd present in the estimates for the modern PM. In the next section, we discuss the implications of our results for the evolution of the HSE in the Archean mantle.

5.3. Constraints on the origin of absolute and relative HSE abundances in the Archean mantle

The observations that the HSE occur in roughly chondritic relative proportions in the upper mantle (Morgan, 1985), and that absolute HSE abundances are two- to four orders of magnitude higher than might be expected based on the low-pressure metal-silicate partitioning data (Morgan et al., 1981) has led to the concept of late accretion. Late accretion is defined for HSE as the addition of ~0.5 wt.% of the mass of the Earth to the mantle after the last major equilibration between the core and mantle (Kimura et al., 1974; Chou et al., 1983). Issues related to late accretion are highly debated, including the time frame within which the bulk of late accreted materials was delivered to Earth, the composition of the late accreted materials, as well as the time frame within which the late accreted materials were homogenized within the mantle. Some of the uncertainties relating to this issue stem from the fact that both the relative and absolute HSE abundances in the Archean mantle are not well constrained, and the causes of apparent variations in the abundances of HSE in the early-Earth mantle are not well understood (see review in Walker (2009) and references therein). For example, on the basis of studies of 3.82 Ga peridotites from West Greenland and 3.46 Ga komatiites from Western Australia, Bennett et al.

(2002) concluded that any HSE-rich components added to the mantle by late accretion must have been transported into and grossly homogenized within the mantle by 3.8 Ga. In contrast to these conclusions, Maier et al. (2009) and Fiorentini et al. (2010), on the basis of their studies of Pt contents in komatiitic lavas of various ages, argued for a gradual increase in the HSE abundances in the terrestrial mantle from ~3.5 to ~2.9 Ga, with little change since ~2.9 Ga. They attributed this increase to the slow, downward mixing of a late veneer of chondritic impactors.

Our present results, considered together with the data for the late Archean komatiite systems compiled from Puchtel and Humayun (2001, 2005), Puchtel et al. (2004a; 2004b), Puchtel et al. (2005), Puchtel et al. (2007) and Puchtel et al. (2009b), indicate that the calculated total absolute Pt and Pd abundances in the Archean mantle sources sampled by komatiites changed little from 3.5 to 2.7 Ga. The one exception, according to our work (Puchtel et al., 2009a), is the 3.55 Ga Schapenburg komatiite system, for which only 27±4% of the total Pt and Pd abundance estimates for the modern PM are calculated. Puchtel et al. (2009a) proposed that the HSE systematics for this komatiite system may have not been set entirely by the addition of chondritic materials after the last major equilibration between the core and the mantle, but also by high-pressure metal-silicate equilibration. A Pt-Os isotopic study of the Schapenburg komatiite system is currently underway and should help clarify this issue.

There are several possible reasons for the discrepancy between our observations and conclusions reached by Maier et al. (2009). First, there is a substantial discrepancy in the absolute concentrations of HSE in sample sets from the localities analyzed here and by Maier et al. (2009). Maier et al. (2009) reported Pt contents, re-calculated for 25% MgO, of ~4.5 ppb and ~7.4 ppb and Ru contents of 2.5 ppb and 4.7 ppb for lavas from the Komati and Weltevreden systems, respectively, whereas the data presented here, when also re-calculated for 25% MgO,

787 indicate ~6.0 and ~11.2 ppb and 3.8 and 6.0 ppb, respectively, as can be seen in **Fig. 3**. We can
788 offer no definitive explanation for this discrepancy at this time, but speculate that it could relate
789 to the differences in analytical methods used or preservation of samples analyzed.
790 Second, of all HSE, Pt and Pd (and Re, where not affected by post-magmatic element
791 mobility) are the elements for which the most robust, and most crucial, source estimates can be
792 obtained. In this study, we show that Pt may have been removed from the sources of some early
793 Archean lavas and added to the sources of others very early in Earth history. Indeed, our study
794 reveals long-term Pt-fractionated nature of the sources of the early Archean komatiite systems
795 compared to their late Archean counterparts (**Fig. 7**), which can greatly affect estimates for the Pt
796 abundances in early Archean komatiite sources.
797 Our results allow us to place additional constraints on the timing of the late accretion. Based
798 on the calculated HSE abundances in the sources of the Komati and Weltevreden systems, these
799 contained between 60 and 70% of the late accreted material complement present in the estimates
800 for the modern PM, and about as much as is present in the sources of some late Archean
801 komatiite systems. If our model is correct and the $^{186}Os/^{188}Os$ isotopic anomalies present in the
802 sources of the early Archean komatiite systems are the result of early differentiation during the
803 solidification of a primordial magma ocean, then most late accreted material must have been
804 added to and homogenized within the mantle before its solidification, e.g., no later than 4400
805 Ma. This conclusion is consistent with both the ^{182}W isotopic data for the Komati system
806 reported by Touboul et al. (2012), as well as with the coupled ^{182}W-HSE data for the
807 Kostomuksha system that require that the bulk of the late accreted materials were added to and
808 homogenized within the mantle within the first 60 Ma of Earth's history (Touboul et al., 2012).
809

Conclusions

Due to their unique properties not found in many terrestrial materials, komatiites are a powerful tool for studies of early-Earth processes. In this study, we report Pt-Re-Os isotopic and HSE abundance data for well preserved komatiites from the 3.48 Ga Komati and 3.26 Ga Weltevreden Fms. of the Barberton Greenstone Belt in South Africa. The Re-Os data for whole-rock samples and pure olivine and chromite separates yield isochrons with ages of 3484±38 and 3263±12 Ma that are consistent with the accepted respective emplacement ages of the Komati and Weltevreden Fms. The calculated initial $^{187}Os/^{188}Os$ = 0.10335±15 ($\gamma^{187}Os$ = +0.34±0.15) and 0.10442±4 ($\gamma^{187}Os$ = -0.14±0.04) for the Komati and Weltevreden systems, respectively, are within the chondritic range. When considered together with the Re-Os data for late Archean komatiite systems, our data indicate that Archean mantle evolved with essentially chondritic time-integrated Re/Os. In constrast, the initial $^{186}Os/^{188}Os$ = 0.1198283±9 ($\varepsilon^{186}Os$ = -0.12±0.08) and 0.1198330±8 ($\varepsilon^{186}Os$ = +0.22±0.07) for the Komati and Weltevreden systems, respectively, are non-chondritic, indicating that mantle sources of these komatiites evolved with fractionated time-integrated Pt/Os.

Our new $^{186,187}Os$ isotopic data for the early Archean komatiite systems, combined with the $^{142,143}Nd$ and ^{176}Hf isotopic data of Puchtel et al. (2013), are consistent with formation, followed by long-term isolation, of deep-seated mantle domains with fractionated time-integrated Sm/Nd, Lu/Hf, and Pt/Os ratios, at ca. 4400 Ma. These domains were likely generated as a result of crystallization of a primordial magma ocean, with Mg-perovskite, Ca-perovskite, and Fe-Pt alloy acting as the fractionating phases. The inferred mantle domains remained isolated from the convecting mantle for at least 1.3 billion years, but were largely mixed away by 2.7 Ga on the scale of mantle reservoirs sampled by late Archean komatiite lavas emplaced worldwide, as evidenced by uniform time-integrated Sm/Nd, Lu/Hf, and Pt/Os ratios in late Archean komatiite systems.

The total Pt and Pd abundances in the sources of early Archean komatiite systems, corrected for the inferred Pt fractionation during crystallization of the terrestrial magma ocean, are calculated to be between 60% and 70% of those present in estimates for the modern PM. These are within the range of the total HSE abundances present in the sources of late Archean komatiite systems, indicating little change in HSE abundances in the Archean mantle between 3.5 and 2.7 Ga.

Higher Pt abundances in late Archean komatiites, compared to their early Archean counterparts, have been taken as evidence for sluggish, downward mixing of late accreted material into the mantle (Maier et al., 2009; Fiorentini et al., 2011). Our new isotopic and HSE abundance data for early Archean komatiite systems are inconsistent with such a scenario. Instead, our data require that late accretion of HSE to Earth was largely complete by the time the terrestrial magma ocean had crystallized. Rather than downward mixing of an HSE-rich late veneer, the Pt concentration variations observed in early Archean komatiites may reflect sluggish mixing of diverse post-magma ocean domains characterized by variably fractionated both lithophile element and HSE abundances.

Acknowledgements

We thank V. Kevlich for the fantastic job with mineral separation and handpicking. The analytical work at the *IGL* was supported by the US National Science Foundation Grant EAR-0946629 to I.S. Puchtel; this support is gratefully acknowledged.

References

Alves, S., Schiano, P., Allegre, C.J., 1999. Rhenium-osmium isotopic investigation of Java subduction zone lavas. Earth and Planetary Science Letters 168 (1-2), 65-77.

Armstrong, R.A., Compston, W., DeWit, M.J., Williams, I.S., 1990. The stratigraphy of the 3.5-3.2 Ga Barberton greenstone belt revisited: A single zircon ion microprobe study. Earth and Planetary Science Letterrs 101 (1), 90-106.

Arndt, N.T., 1977. Ultrabasic magmas and high-degree melting of the mantle. Contributions to Mineralogy and Petrology 64 (2), 205-221.

Arndt, N.T., Lesher, C.M., Barnes, S.J., 2008. Komatiite. Cambridge, UK, Cambridge University Press.

Barnes, S.-J., Naldrett, A.J., Gorton, M.P., 1985. The origin of the fractionation of platinum-group elements in terrestrial magmas. Chemical Geology 53 (3-4), 303-323.

Barnes, S.J., Fiorentini, M.L., 2008. Iridium, ruthenium and rhodium in komatiites: Evidence for iridium alloy saturation. Chemical Geology 257 (1-2), 44-58.

Becker, H., Horan, M.F., Walker, R.J., Gao, S., Lorand, J.-P., Rudnick, R.L., 2006. Highly siderophile element composition of the Earth's primitive upper mantle: Constraints from new data on peridotite massifs and xenoliths. Geochimica et Cosmochimica Acta 70 (17), 4528-4550.

Begemann, F., Ludwig, K.R., Lugmair, G.W., Min., K., Nyquist, L.E., Patchett, P.J., Renne, P.R., Shih, C.-Y., Villa, I.M., Walker, R.J., 2001. Call for an improved set of decay constants for geochronological use. Geochimica et Cosmochimica Acta 65 (1), 111-121.

Bennett, V.C., Nutman, A.P., Esat, T.M., 2002. Constraints on mantle evolution from $^{187}Os/^{188}Os$ isotopic compositions of Archean ultramafic rocks from southern West Greenland (3.8 Ga) and Western Australia (3.46 Ga). Geochimica et Cosmochimica Acta 66 (14), 2615-2630.

Bezos, A., Lorand, J.-P., Humler, E., Gros, M., 2005. Platinum-group element systematics in Mid-Oceanic Ridge basaltic glasses from the Pacific, Atlantic, and Indian Oceans. Geochimica et Cosmochimica Acta 69 (10), 2613-2627.

Birck, J.L., Roy-Barman, M., Capman, F., 1997. Re-Os isotopic measurements at the femtomole level in natural samples. Geostandards Newsletter 20 (1), 19-27.

Borisov, A., Palme, H., 1997. Experimental determination of the solubility of platinum in silicate melts. Geochimica et Cosmochimica Acta 61 (20), 4349-4357.

Borisov, A., Palme, H., 2000. Solubilities of noble metals in Fe-containing silicate melts as derived from experiments in Fe-free systems. American Mineralogist 85 (11-12), 1665-1673.

Brandon, A.D., Creaser, R.A., Shirey, S.B., Carlson, R.W., 1996. Osmium recycling in subduction zones. Science 272 (5263), 861-864.

Brandon, A.D., Walker, R.J., Morgan, J.W., Norman, M.D., Prichard, H.M., 1998. Coupled ^{186}Os and ^{187}Os evidence for core-mantle interaction. Science 280 (5369), 1570-1573.

Brandon, A.D., Becker, H., Carlson, R.W., Shirey, S.B., 1999. Isotopic constraints on time scales and mechanisms of slab material transport in the mantle wedge: Evidence from the Simcoe mantle xenoliths, Washington, USA. Chemical Geology 160 (4), 387-407.

Brandon, A.D., Snow, J.E., Walker, R.J., Morgan, J.W., Mock, T.D., 2000. ^{190}Pt-^{186}Os and ^{187}Re-^{187}Os systematics of abyssal peridotites. Earth and Planetary Science Letters 177 (3-4), 319-335.

902 Brandon, A.D., Humayun, M., Puchtel, I.S., Zolensky, M., 2005a. Re-Os isotopic systematics
903 and platinum group element composition of the Tagish Lake carbonaceous chondrite.
904 Geochimica et Cosmochimica Acta 69 (6), 1619-1631.
905 Brandon, A.D., Walker, R.J., 2005. The debate over core-mantle interaction. Earth and Planetary
906 Science Letters 232 (3-4), 211-225.
907 Brandon, A.D., Walker, R.J., Puchtel, I.S., Humayun, M., 2005b. Platinum-osmium isotope
908 evolution of the Earth's mantle. Geochimica et Cosmochimica Acta 69, A392.
909 Brandon, A.D., Walker, R.J., Puchtel, I.S., 2006. Platinum-osmium isotope evolution of the
910 Earth's mantle: Constraints from chondrites and Os-rich alloys. Geochimica et
911 Cosmochimica Acta 70 (8), 2093-2103.
912 Brenan, J.M., McDonough, W.F., Dalpé, C., 2003. Experimental constraints on the partitioning
913 of rhenium and some platinum-group elements between olivine and silicate melt. Earth
914 and Planetary Science Letters 212 (1-2), 135-150.
915 Brenan, J.M., McDonough, W.F., Ash, R., 2005. An experimental study of the solubility and
916 partitioning of iridium, osmium, and gold between olivine and silicate melt. Earth and
917 Planetary Science Letters 237 (3-4), 855-872.
918 Brenan, J.M., 2008. Re-Os fractionation by sulfide melt-silicate melt partitioning: A new spin.
919 Chemical Geology 248 (3-4), 140-165.
920 Brenan, J.M., Finnigan, C.F., McDonough, W.F., Homolova, V., 2012. Experimental constraints
921 on the partitioning of Ru, Rh, Ir, Pt and Pd between chromite and silicate melt: The
922 importance of ferric iron. Chemical Geology 302-303, 16-32.
923 Brügmann, G.E., Arndt, N.T., Hofmann, A.W., Tobschall, H.J., 1987. Noble metal abundances
924 in komatiite suites from Alexo, Ontario, and Gorgona Island, Colombia. Geochimica et
925 Cosmochimica Acta 51 (8), 2159-2169.
926 Campbell, I.H., Griffiths, R.W., Hill, R.I., 1989. Melting in an Archaean mantle plume: head it's
927 basalts, tails it's komatiites. Nature 339 (6227), 697-699.
928 Chou, C.-L., Shaw, D.M., Crocket, J.H., 1983. Siderophile trace elements in the Earth's oceanic
929 crust and upper mantle. Journal of Geophysical Research 88 (S2), A507-A518.
930 Cohen, A.S., Waters, F.G., 1996. Separation of osmium from geological materials by solvent
931 extraction for analysis by thermal ionisation mass spectrometry. Analytica Chimica Acta
932 332 (2-3), 269-275.
933 Colodner, D.C., Boyle, E.A., Edmond, J.M., Thomson, J., 1992. Post-depositional mobility of
934 platinum, iridium and rhenium in marine sediments. Nature 358 (6385), 402-404.
935 Connolly, B.D., Puchtel, I.S., Walker, R.J., Arevalo, R.J., Piccoli, P.M., Byerly, G.R., Robin-
936 Popieul, C., Arndt, N.T., 2011. Highly Siderophile Element systematics of the 3.3 Ga
937 Weltevreden komatiites, South Africa: implications for early Earth history. Earth and
938 Planetary Science Letters 311 (3-4), 253-263.
939 Creaser, R.A., Papanastassiou, D.A., Wasserburg, G.J., 1991. Negative Thermal Ion Mass-
940 Spectrometry of Osmium, Rhenium, and Iridium. Geochimica et Cosmochimica Acta 55
941 (1), 397-401.
942 Crocket, J.H., MacRae, W.E., 1986. Platinum-group element distribution in komatiitic and
943 tholeiitic volcanic rocks from Munro Township, Ontario. Economic Geology 81 (5),
944 1242-1251.
945 Dann, J.C., 2000. The 3.5 Ga Komati Formation, Barberton Greenstone Belt, South Africa, Part
946 I: New maps and magmatic architecture. South African Journal of Geology 103 (1), 47-
947 68.

948 Fiorentini, M.L., Barnes, S.J., Maier, W.D., Burnham, O.M., Heggie, G., 2010. Global
949 Variability in the Platinum-group Element Contents of Komatiites. Journal of Petrology
950 52 (1), 83-112.
951 Fiorentini, M.L., Barnes, S.J., Maier, W.D., Burnham, O.M., Heggie, G., 2011. Global
952 Variability in the Platinum-group Element Contents of Komatiites. Journal of Petrology
953 52 (1), 83-112.
954 Fischer-Gödde, M., Becker, H., Wombacher, F., 2011. Rhodium, gold and other highly
955 siderophile elements in orogenic peridotites and peridotite xenoliths. Chemical Geology
956 280 (3-4), 365-383.
957 Fonseca, R.O.C., Mallmann, G., O'Neill, H.S.C., Campbell, I.H., 2007. How chalcophile is
958 rhenium? An experimental study of the solubility of Re in sulphide mattes. Earth and
959 Planetary Science Letters 260 (3-4), 537-548.
960 Fonseca, R.O.C., Mallmann, G., O'Neill, H.S.C., Campbell, I.H., Laurenz, V., 2011. Solubility of
961 Os and Ir in sulfide melt: Implications for Re/Os fractionation during mantle melting.
962 Earth and Planetary Science Letters 311 (3-4), 339-350.
963 Fonseca, R.O.C., Laurenz, V., Mallmann, G., Luguet, A., Hoehne, N., Jochum, K.P., 2012. New
964 constraints on the genesis and long-term stability of Os-rich alloys in the Earth's mantle.
965 Geochimica et Cosmochimica Acta 87, 227-242.
966 Foster, J.G., Lambert, D.D., Frick, L.R., Maas, R., 1996. Re-Os isotopic evidence for genesis of
967 Archaean nickel ores from uncontaminated komatiites. Nature 382 (6593), 703-706.
968 Frost, D.J., Liebske, C., Langenhorst, F., McCammon, C.A., Trønnes, R.G., Rubie, D.C., 2004.
969 Experimental evidence for the existence of iron-rich metal in the Earth's lower mantle.
970 Nature 428 (6981), 409-412.
971 Frost, D.J., Mann, U., Asahara, Y., Rubie, D.C., 2008. The redox state of the mantle during and
972 just after core formation. Philosophical Transactions of the Royal Society a-Mathematical
973 Physical and Engineering Sciences 366 (1883), 4315-4337.
974 Frost, D.J., McCammon, C.A., 2008. The redox state of Earth's mantle. In: (Ed.), Annual
975 Review of Earth and Planetary Sciences. Annual Reviews, Palo Alto, 36, 389-420.
976 Gangopadhyay, A., Walker, R.J., 2003. Re-Os systematics of the ca. 2.7 Ga komatiites from
977 Alexo, Ontario, Canada. Chemical Geology 196 (1-4), 147-162.
978 Gangopadhyay, A., Sproule, R.A., Walker, R.J., Lesher, C.M., 2005. Re-Os systematics of
979 komatiites and komatiitic basalts at Dundonald Beach, Ontario, Canada: Evidence for a
980 complex alteration history and implications of a late-Archean chondritic mantle source.
981 Geochimica et Cosmochimica Acta 69 (21), 5087-5098.
982 Gangopadhyay, A., Walker, R.J., Hanski, E., Solheid, P., 2006. Origin of Paleoproterozoic
983 Komatiites at Jeesiörova, Kittilä Greenstone Complex, Finnish Lapland. Journal of
984 Petrology 47 (4), 773-789.
985 Hamlyn, P.R., Keays, R.R., Cameron, W.E., Crawford, A.J., Waldron, H.M., 1985. Precious
986 metals in magnesian low-Ti lavas: Implications for metallogenesis and sulfur saturation
987 in primary magmas. Geochimica et Cosmochimica Acta 49 (8), 1797-1811.
988 Handler, M.R., Bennett, V.C., 1999. Behaviour of platinum-group elements in the subcontinental
989 mantle of eastern Australia during variable metasomatism and melt depletion.
990 Geochimica et Cosmochimica Acta 63 (21), 3597-3618.
991 Hanski, E., Walker, R.J., Huhma, H., Polyakov, G.V., Balykin, P.A., Hoa, T.T., Phuong, N.T.,
992 2004. Origin of the Permian-Triassic komatiites, northwestern Vietnam. Contributions to
993 Mineralogy and Petrology 147 (4), 453-469.

Hauri, E.H., Hart, S.R., 1993. Re-Os isotope systematics of HIMU and EMII oceanic island basalts from the south Pacific Ocean. Earth and Planetary Science Letters 114 (2-3), 353-371.

Horan, M.F., Walker, R.J., Morgan, J.W., Grossman, J.N., Rubin, A.E., 2003. Highly siderophile elements in chondrites. Chemical Geology 196 (1-4), 5-20.

Humayun, M., 2011. A model for osmium isotopic evolution of metallic solids at the core-mantle boundary. Geochemistry Geophysics Geosystems 12.

Huppert, H.E., Sparks, R.S.J., 1985. Cooling and contamination of mafic and ultramafic magmas during ascent through continental crust. Earth and Planetary Science Letterrs 74 (4), 371-386.

Kareem, K. (2005). Komatiites of the Weltevreden Formation, Barberton Greenstone Belt, South Africa: Implications for the chemistry and temperature of the Archean mantle. Department of Geology and Geophysics. Baton Rouge, Louisiana State University. **Doctor of Philosophy:** 233.

Keays, R.R., 1995. The role of komatiitic and picritic magmatism and S-saturation in the formation of ore deposits. Lithos 34 (1-3), 1-18.

Kimura, K., Lewis, R.S., Anders, S., 1974. Distribution of gold and rhenium between nickel-iron and silicate melts; implications for abundance of siderophile elements on the earth and moon. Geochimica et Cosmochimica Acta 38 (5), 683-701.

Lassiter, J.C., Hauri, E.H., 1998. Osmium-isotope variations in Hawaiian lavas: evidence for recycled oceanic lithosphere in the Hawaiian plume. Earth and Planetary Science Letters 164 (3-4), 483-496.

Liu, C.Z., Snow, J.E., Brugmann, G., Hellebrand, E., Hofmann, A.W., 2009. Non-chondritic HSE budget in Earth's upper mantle evidenced by abyssal peridotites from Gakkel ridge (Arctic Ocean). Earth and Planetary Science Letters 283 (1-4), 122-132.

Lorand, J.-P., Pattou, L., Gros, M., 1999. Fractionation of platinum-group elements and gold in the upper mantle: a detailed study in Pyrenean Orogenic lherzolites. Journal of Petrology 40 (6), 957-981.

Lorand, J.-P., Alard, O., 2001. Platinum-group element abundances in the upper mantle: new constraints from in situ and whole-rock analyses of Massif Central xenoliths (France). Geochimica et Cosmochimica Acta 65 (16), 2789-2806.

Lorand, J.P., Alard, O., Godard, M., 2009. Platinum-group element signature of the primitive mantle rejuvenated by melt-rock reactions: evidence from Sumail peridotites (Oman Ophiolite). Terra Nova 21 (1), 35-40.

Lowe, D.R., 1994. Accretionary history of the Archean Barberton Greenstone Belt (3.55-3.22 Ga), southern Africa. Geology 22 (12), 1099-1102.

Lowe, D.R., 1999. Geologic evolution of the Barberton Greenstone Belt and vicinity. In: Lowe, D.R. and Byerly, G.R. (Ed.), Geological Evolution of the Barberton Greenstone Belt. Geological Society of America, Special Paper 329, Boulder, 287-312.

Lowe, D.R., Byerly, G.R., 1999. Stratigraphy of the west-central part of the Barberton Greenstone Belt, South Africa. In: Lowe, D.R. and Byerly, G.R. (Ed.), Geological Evolution of the Barberton Greenstone Belt. Geological Society of America, Special Paper 329, Boulder, 1-36.

Lowe, D.R., Byerly, G.R., 2007. An overview of the geology of the Barberton Greenstone Belt and vicinity: Implications for early crustal development. In: Van Kranendonk, M.J.,

Smithies, R.H., and Bennett, V.C. (Ed.), Earth's Oldest Rocks. Elsevier, Amsterdam, 15, 481-526.
Ludwig, K.R. (2003). ISOPLOT 3.00. A geochronological toolkit for Microsoft Excel. Berkeley Geochronology Center Spec. Publ. **No. 4:** 70 pp.
Luguet, A., Lorand, J.-P., Seyler, M., 2003. Sulfide petrology and highly siderophile element geochemistry of abyssal peridotites: a coupled study of samples from the Kane Fracture Zone (45°W 23°20N, Mark Area, Atlantic Ocean). Geochimica et Cosmochimica Acta 67 (8), 1553-1570.
Luguet, A., Shirey, S.B., Lorand, J.-P., Horan, M.F., Carlson, R.W., 2007. Residual platinum-group minerals from highly depleted harzburgites of the Lherz massif (France) and their role in HSE fractionation of the mantle. Geochimica et Cosmochimica Acta 71 (12), 3082-3097.
Maier, W.D., Roelofse, F., Barnes, S.J., 2003. The concentration of the platinum-group elements in south African komatiites: Implications for mantle sources, melting regime and PGE fractionation during crystallization. Journal of Petrology 44 (10), 1787-1804.
Maier, W.D., Barnes, S.J., Campbell, I.H., Fiorentini, M.L., Peltonen, P., Barnes, S.J., Smithies, R.H., 2009. Progressive mixing of meteoritic veneer into the early Earth's deep mantle. Nature 460 (7255), 620-623.
Mavrogenes, J.A., O'Neill, H.S.C., 1999. The relative effects of pressure, temperature and oxygen fugacity on the solubility of sulfide in mafic magmas. Geochimica et Cosmochimica Acta 63 (7-8), 1173-1180.
McDonough, W.F., Sun, S.S., 1995. The composition of the Earth. Chemical Geology 120 (3-4), 223-253.
Meisel, T., Walker, R.J., Irving, A.J., Lorand, J.-P., 2001. Osmium isotopic compositions of mantle xenoliths: A global perspective. Geochimica et Cosmochimica Acta 65 (8), 1311-1323.
Meisel, T., Reisberg, L., Moser, J., Carignan, J., Melcher, F., Brügmann, G., 2003. Re-Os systematics of UB-N, a serpentinized peridotite reference material. Chemical Geology 201 (1-2), 161-179.
Meisel, T., Moser, J., 2004. Reference materials for geochemical PGE analysis: new analytical data for Ru, Rh, Pd, Os, Ir, Pt, and Re by isotope dilution ICP-MS in 11 geological reference materials. Chemical Geology 208 (1-4), 319-338.
Morgan, J.W., Wanderless, G.A., Petrie, R.K., Irving, A.J., 1981. Composition of the earth's upper mantle, I. Siderophile trace elements in ultramafic nodules. Tectonophysics 75 (1-2), 47-67.
Morgan, J.W., 1985. Osmium isotope constraints on Earth's late accretionary history. Nature 317 (6039), 703-705.
Morgan, J.W., 1986. Ultramafic xenoliths: Clues to Earth's late accretionary history. Journal of Geophysical Research 91 (B12), 12375-12387.
Peach, C.L., Mathez, E.A., Keays, R.R., 1990. Sulfide melt-silicate melt distribution coefficients for noble metals and other chalcophile elements as deduced from MORB; implications for partial melting. Geochimica et Cosmochimica Acta 54 (12), 3379-3389.
Pearson, D.G., Irvine, G.J., Ionov, D.A., Boyd, F.R., Dreibus, G.E., 2004. Re-Os isotope systematics and platinum-group-element fractionation during mantle melt extraction: A study of massif and xenolith peridotite suites. Chemical Geology 208, 29-59.

1084 Penniston-Dorland, S.C., Walker, R.J., Pitcher, L., Sorensen, S.S., 2012. Mantle-crust
1085 interactions in a paleosubduction zone: Evidence from highly siderophile element
1086 systematics of eclogite and related rocks. Earth and Planetary Science Letters 319, 295-
1087 306.
1088 Puchtel, I., Humayun, M., 2000. Platinum group elements in Kostomuksha komatiites and
1089 basalts: Implications for oceanic crust recycling and core-mantle interaction. Geochimica
1090 et Cosmochimica Acta 64 (24), 4227-4242.
1091 Puchtel, I.S., Haase, K.M., Hofmann, A.W., Chauvel, C., Kulikov, V.S., Garbe-Schönberg, C.D.,
1092 Nemchin, A.A., 1997. Petrology and geochemistry of crustally contaminated komatiitic
1093 basalts from the Vetreny Belt, southeastern Baltic Shield: Evidence for an early
1094 Proterozoic mantle plume beneath rifted Archean continental lithosphere. Geochimica et
1095 Cosmochimica Acta 61 (6), 1205-1222.
1096 Puchtel, I.S., Hofmann, A.W., Mezger, K., Jochum, K.P., Shchipansky, A.A., Samsonov, A.V.,
1097 1998. Oceanic plateau model for continental crustal growth in the Archaean: A case study
1098 from the Kostomuksha greenstone belt, NW Baltic Shield. Earth and Planetary Science
1099 Letters 155 (1-2), 57-74.
1100 Puchtel, I.S., Hofmann, A.W., Amelin, Y.V., Garbe-Schönberg, C.-D., Samsonov, A.V.,
1101 Shchipansky, A.A., 1999. Combined mantle plume - island arc model for the formation
1102 of the 2.9 Ga Sumozero-Kenozero greenstone belt, SE Baltic Shield: Isotope and trace
1103 element constraints. Geochimica et Cosmochimica Acta 63 (21), 3579-3595.
1104 Puchtel, I.S., Brügmann, G.E., Hofmann, A.W., 2001a. ^{187}Os-enriched domain in an Archaean
1105 mantle plume: Evidence from 2.8 Ga komatiites of the Kostomuksha greenstone belt,
1106 NW Baltic Shield. Earth and Planetary Science Letters 186 (3-4), 513-526.
1107 Puchtel, I.S., Brügmann, G.E., Hofmann, A.W., Kulikov, V.S., Kulikova, V.V., 2001b. Os
1108 isotope systematics of komatiitic basalts from the Vetreny belt, Baltic Shield: Evidence
1109 for a chondritic source of the 2.45 Ga plume. Contributions to Mineralogy and Petrology
1110 140 (5), 588-599.
1111 Puchtel, I.S., Humayun, M., 2001. Platinum group element fractionation in a komatiitic basalt
1112 lava lake. Geochimica et Cosmochimica Acta 17 (65), 2979-2993.
1113 Puchtel, I.S., Brandon, A.D., Humayun, M., 2004a. Precise Pt-Re-Os isotope systematics of the
1114 mantle from 2.7-Ga komatiites. Earth and Planetary Science Letters 224 (1-2), 157-174.
1115 Puchtel, I.S., Humayun, M., Campbell, A., Sproule, R., Lesher, C.M., 2004b. Platinum group
1116 element geochemistry of komatiites from the Alexo and Pyke Hill areas, Ontario,
1117 Canada. Geochimica et Cosmochimica Acta 68 (6), 1361-1383.
1118 Puchtel, I.S., Brandon, A.D., Humayun, M., Walker, R.J., 2005. Evidence for the early
1119 differentiation of the core from Pt-Re-Os isotope systematics of 2.8-Ga komatiites. Earth
1120 and Planetary Science Letters 237 (1-2), 118-134.
1121 Puchtel, I.S., Humayun, M., 2005. Highly siderophile element geochemistry of ^{187}Os-enriched
1122 2.8-Ga Kostomuksha komatiites, Baltic Shield. Geochimica et Cosmochimica Acta 69
1123 (6), 1607-1618.
1124 Puchtel, I.S., Humayun, M., Walker, R.J., 2007. Os-Pb-Nd isotope and highly siderophile and
1125 lithophile trace element systematics of komatiitic rocks from the Volotsk suite, SE Baltic
1126 Shield. Precambrian Research 158 (1-2), 119-137.
1127 Puchtel, I.S., Walker, R.J., Anhaeusser, C.R., Gruau, G., 2009a. Re-Os isotope systematics and
1128 HSE abundances of the 3.5 Ga Schapenburg komatiites, South Africa: Hydrous melting

or prolonged survival of primordial heterogeneities in the mantle? Chemical Geology 262 (3-4), 355-369.
Puchtel, I.S., Walker, R.J., Brandon, A.D., Nisbet, E.G., 2009b. Pt-Re-Os and Sm-Nd isotope and HSE and REE systematics of the 2.7 Ga Belingwe and Abitibi komatiites. Geochimica et Cosmochimica Acta 73 (20), 6367-6389.
Puchtel, I.S., Blichert-Toft, J., Touboul, M., Walker, R.J., Byerly, G., Nisbet, E.G., Anhaeusser, C.R., 2013. Insights into early Earth from Barberton komatiites: Evidence from lithophile isotope and trace element systematics. Geochimica et Cosmochimica Acta 108, 63-90.
Rehkämper, M., Halliday, A.N., 1997. Development and application of new ion-exchange techniques for the separation of the platinum-group and other siderophile elements from geological samples. Talanta 44 (4), 663-672.
Rehkämper, M., Halliday, A.N., Barfod, D., Fitton, J.G., 1997. Platinum-group element abundance patterns in different mantle environments. Science 278 (5343), 1595-1598.
Rehkämper, M., Halliday, A.N., Alt, J., Fitton, J.G., Zipfel, J., Takazawa, E., 1999a. Non-chondritic platinum-group element ratios in oceanic mantle lithosphere: petrogenetic signature of melt percolation? Earth and Planetary Science Letters 172 (1-2), 65-81.
Rehkämper, M., Halliday, A.N., Fitton, J.G., Lee, D.-C., Wieneke, M., Arndt, N.T., 1999b. Ir, Ru, Pt and Pd in basalts and komatiites: New constraints for the geochemical behavior of the platinum group elements in the mantle. Geochimica et Cosmochimica Acta 63 (22), 3915-3934.
Reisberg, L., Lorand, J.-P., 1995. Longevity of subcontinental mantle lithosphere from osmium isotope systematics in orogenic peridotite massifs. Nature 376 (6536), 159-162.
Righter, K., 2003. Metal-silicate partitioning of siderophile elements and core formation in the early Earth. Annual Review of Earth and Planetary Sciences 31, 135-174.
Shirey, S.B., Lewin, K.W., Berg, J.H., Carlson, R.W., 1994. Temporal changes in the sources of flood basalts: Isotopic and trace element evidence from the 1100 Ma old Keweenawan Mamainse Point Formation, Ontario, Canada. Geochimica et Cosmochimica Acta 58 (20), 4475-4490.
Shirey, S.B., 1997. Re-Os isotopic compositions of midcontinent rift system picrites: implications for plume-lithosphere interaction and enriched mantle sources. Canadian Journal of Earth Sciences 34 (4), 489-503.
Shirey, S.B., Walker, R.J., 1998. The Re-Os isotope system in cosmochemistry and high-temperature geochemistry. Annual Reviews of Earth and Planetary Sciences 26, 423-500.
Smoliar, M.I., Walker, R.J., Morgan, J.W., 1996. Re-Os ages of Group IIA, IIIA, IVA, and IVB iron meteorites. Science 271 (5762), 1099-1102.
Snow, J.E., Reisberg, L., 1995. Os isotopic systematics of the MORB mantle: Results from altered abyssal peridotites. Earth and Planetary Science Letters 136 (3-4), 723-733.
Stiegler, M.T., Cooper, M., Byerly, G.R., Lowe, D.R., 2012. Geochemistry and petrology of komatiites of the Pioneer Ultramafic Complex of the 3.3 Ga Weltevreden Formation, Barberton greenstone belt, South Africa. Precambrian Research 212, 1-12.
Touboul, M., Puchtel, I.S., Walker, R.J., 2012. ^{182}W Evidence for Long-Term Preservation of Early Mantle Differentiation Products. Science 335, 1065-1069.
Tsuru, A., Walker, R.J., Kontinen, A., Peltonen, P., Hanski, E., 2000. Re-Os isotopic systematics of the 1.95 Ga Jormua Ophiolite Complex, northeastern Finland. Chemical Geology 164 (1-2), 123-141.

1174 Viljoen, M.J., Viljoen, R.P., 1969. The geology and geochemistry of the Lower Ultramafic Unit
1175 of the Onverwacht Group and a proposed new class of igneous rocks. Geological Society
1176 of South Africa Special Publication 2, 55-86.
1177 Viljoen, M.J., Viljoen, R.P., Smith, H.S., Erlank, A.J., 1983. Geological, textural and
1178 geochemical features of komatiitic flows from the Komati Formation. Geol. Soc. South
1179 Africa Spec. Publ. 9, 1-20.
1180 Wade, J., Wood, B.J., 2005. Core formation and the oxidation state of the Earth. Earth and
1181 Planetary Science Letters 236 (1-2), 78-95.
1182 Walker, R.J., Shirey, S.B., Stecher, O., 1988. Comparative Re-Os, Sm-Nd and Rb-Sr isotope and
1183 trace element systematics for Archean komatiite flows from Munro Township, Abitibi
1184 belt, Ontario. Earth and Planetary Science Letters 87 (1-2), 1-12.
1185 Walker, R.J., Carlson, R.W., Shirey, S.B., Boyd, F.R., 1989. Os, Sr, Nd, and Pb isotope
1186 systematics of southern African peridotite xenoliths: Implications for the chemical
1187 evolution of subcontinental mantle. Geochimica et Cosmochimica Acta 53 (7), 1583-
1188 1595.
1189 Walker, R.J., Echeverria, L.M., Shirey, S.B., Horan, M.F., 1991. Re-Os isotopic constraints on
1190 the origin of volcanic rocks, Gorgona Island, Colombia: Os-isotopic evidence for ancient
1191 heterogeneities in the mantle. Contributions to Mineralogy and Petrology 107 (2), 150-
1192 162.
1193 Walker, R.J., Morgan, J.W., Horan, M.F., 1995. ^{187}Os enrichment in some plumes: evidence for
1194 core-mantle interaction? Science 269 (5225), 819-822.
1195 Walker, R.J., Hanski, E., Vuollo, J., Liipo, J., 1996. The Os isotopic composition of Proterozoic
1196 upper mantle: evidence for chondritic upper mantle from the Outokumpu ophiolite,
1197 Finland. Earth and Planetary Science Letters 141 (1-4), 161-173.
1198 Walker, R.J., Morgan, J.W., Beary, E.S., Smoliar, M.I., Czamanske, G.K., Horan, M.F., 1997.
1199 Applications of the ^{190}Pt-^{186}Os isotope system to geochemistry and cosmochemistry.
1200 Geochimica et Cosmochimica Acta 61 (22), 4799-4807.
1201 Walker, R.J., Storey, M., Kerr, A.C., Tarney, J., Arndt, N.T., 1999. Implications of ^{187}Os isotopic
1202 heterogeneities in a mantle plume: Evidence from Gorgona Island and Curaçao.
1203 Geochimica et Cosmochimica Acta 63 (5), 713-728.
1204 Walker, R.J., Stone, W.E., 2001. Os isotope constraints on the origin of the 2.7 Ga Boston Creek
1205 Flow, Ontario, Canada. Chemical Geology 175 (3-4), 567-579.
1206 Walker, R.J., Prichard, H.M., Ishivatari, A., Pimentel, M., 2002. The osmium isotopic
1207 composition of the convecting upper mantle deduced from ophiolite chromites.
1208 Geochimica et Cosmochimica Acta 66 (2), 329-345.
1209 Walker, R.J., Brandon, A.D., Bird, J.M., Piccoli, P.M., McDonough, W.F., Ash, R.D., 2005.
1210 ^{187}Os-^{186}Os systematics of Os-Ir-Ru alloy grains from southwestern Oregon. Earth and
1211 Planetary Science Letterrs 230 (1-2), 211-226.
1212 Walker, R.J., 2009. Highly siderophile elements in the Earth, Moon and Mars: Update and
1213 implications for planetary accretion and differentiation. Chemie der Erde - Geochemistry
1214 69 (2), 101-125.
1215 Wilson, A.H., Shirey, S.B., Carlson, R.W., 2003. Archaean ultra-depleted komatiites formed by
1216 hydrous melting of cratonic mantle. Nature 423 (6942), 858-860.
1217 Woodland, S.J., Pearson, D.G., Thirlwall, M.F., 2002. A platinum-group element and Re-Os
1218 isotope investigation of siderophile element recycling in subduction zones: Comparison

of Grenada, Lesser Antilles Arc, and the Izu-Bonin Arc. Journal of Petrology 43 (1), 171-198.

Figure captions

Figure 1. Re-Os isochron diagrams for the Komati (upper panel) and Weltevreden Fm. (lower panel) komatiites. The data set for the latter include both our data and those reported by Connolly et al. (2011), as discussed in the text. Two cumulate samples (BV14 from Komati and SA501-7 from Weltevreden) plot well below the respective regression lines and were excluded from the regression calculations for reasons discussed in the text. The uncertainties on the ages and the initial isotopic ratios ($2\sigma_{mean}$) are derived from the ISOPLOT regression calculations.

Figure 2. Pt-Os isotopic data for the Komati (upper panel) and Weltevreden (lower panel) komatiite systems. The initial $^{186}Os/^{188}Os$ ratios represent averages of the initial $^{186}Os/^{188}Os$ ratios for each individual sample analyzed calculated using measured $^{186}Os/^{188}Os$ and $^{190}Pt/^{188}Os$. The uncertainties on the average initial $^{186}Os/^{188}Os$ ratios for each system are determined by the external long-term reproducibility for the in-house Johnson-Matthey Os standard (±14 ppm) divided by square root of the number of samples analyzed for each system. The chondritic reference lines for the respective emplacement ages of 3484 Ma and 3263 Ma are constructed on the basis of parameters from Brandon et al. (2006), as discussed in the text.

Figure 3. Variations of HSE abundances as a function of MgO contents in the Komati and Weltevreden whole-rock komatiite samples and pure olivine separates. The regression lines were fitted through the whole-rock and olivine separate data using ISOPLOT. The samples that plot off the regression lines were not included into the regression calculations.

Figure 4. Normalized to an average CI chondrite Orgueil (Horan et al., 2003) HSE abundances in whole-rock komatiite samples from the Komati (upper left panel) and Weltevreden (lower left panel) Fms., as well as in the calculated emplaced komatiite lavas from both localities (upper right panel).

Figure 5. Normalized to an average CI chondrite Orgueil (Horan et al., 2003) HSE abundances in olivine (upper panel) and chromite (lower panel) separates from the Komati and Weltevreden komatiites.

Figure 6a. Initial $^{187}Os/^{188}Os$ isotopic compositions, expressed in $\gamma^{187}Os$ terms, of best studied Archean komatiite systems, and of olivine and chromite separates from Isua peridotites, plotted as a function of age. The $^{187}Os/^{188}Os$ isotopic data for the komatiite systems are from Foster et al. (1996), Puchtel et al. (2001a; 2001b), Puchtel et al. (2004a), Puchtel et al. (2005), Puchtel et al. (2007), Puchtel et al. (2009a; 2009b) and this study, and for the Isua peridotites – from Bennett et al. (2002). These data are compared with those for the average PM estimate from Meisel et al. (2001), and with the data for an average abyssal peridotite from Snow and Reisberg (1995), Brandon et al. (2000), and Liu et al. (2009). **b.** Initial $^{186}Os/^{188}Os$ isotopic compositions, expressed in $\varepsilon^{186}Os$ terms, of Archean komatiite systems studied to-date, plotted as a function of age. The $^{186}Os/^{188}Os$ isotopic data for the komatiite

systems are from Puchtel et al. (2004a), Puchtel et al. (2005), Puchtel et al. (2009b) and this study. The parameters for the model PM reservoir were adopted from Brandon et al. (2006) and for the model DMM reservoir – from Brandon et al. (2000). The uncertainties on the Os initial isotopic ratios are $2\sigma_{mean}$.

Figure 7. Normalized to an average CI chondrite Orgueil (Horan et al., 2003) HSE abundances in the sources of the Komati and Weltevreden komatiite systems calculated using the projection technique of Puchtel et al. (2004b) and Puchtel and Humayun (2005) described in the text, and in an average Komati-Weltevreden komatiite source. The Pt abundances are corrected for Pt-Fe alloy fractionation, as discussed in the text. The average late Archean komatiite source from Puchtel et al. (2009b) and a PM estimate of Becker et al. (2006) are plotted for comparison. The uncertainties are $2\sigma_{mean}$.

Figure 8. Calculated total Pt and Pd abundances in the sources of the Komati and Weltevreden komatiite systems from this study plotted as a per cent of the total Pt and Pd abundances in the estimates of the modern PM of Becker et al. (2006). In the calculations of the totals, the relative weight of Pd contribution to the total was normalized to Pt on the basis of its relative abundance in an average CI chondrite Orgueil (Horan et al., 2003). The total Pt and Pd abundances present in the sources of the best-studied late Archean komatiite systems compiled from the data of Puchtel and Humayun (2001, 2005), Puchtel et al. (2004a; 2004b), Puchtel et al. (2005), Puchtel et al. (2007), and Puchtel et al. (2009b) and for the 3.55 Ga Schapenburg komatiite system from Puchtel et al. (2009a) are plotted for comparison. The uncertainties are $2\sigma_{mean}$.

Table 1. HSE abundances (ppb) and $^{187}Os/^{188}Os$ ratios in the UB-N and GP-13 reference materials.

Lab	*n*	Re	Os	Ir	Ru	Pt	Pd	$^{187}Os/^{188}Os$
UB-N								
IGL [1]	5	0.211±0.010	3.79±0.27	3.55±0.32	6.88±0.37	7.71±0.07	6.10±0.10	0.12706±16
IGL [2]	4	0.205±0.004	3.51±0.12	3.26±0.13	6.51±0.33	7.00±0.23	5.85±0.26	0.12737±25
Chicago [3]	6	0.199±0.023	3.72±0.35	3.62±0.22	7.42±0.52	7.52±0.27	6.11±0.23	
Leoben [4]	14	0.210±0.004	3.85±0.13	3.38±0.22	6.30±0.30	7.42±0.30	6.11±0.18	
GP-13								
IGL [1]	6	0.307±0.010	3.77±0.11	3.52±0.25	6.89±0.09	7.54±0.34	5.92±0.16	0.12644±9
Chicago [3]	3	0.283±0.003	3.70±0.02	3.42±0.08	7.03±0.38	6.82±0.48	5.34±0.10	
Leoben [4]	7	0.312±0.023	4.06±0.07	3.40±0.18	6.05±0.95	6.38±1.09	5.80±0.36	
Durham [5]	8	0.330±0.007	3.87±0.24	3.56±0.46	6.97±0.33	7.00±0.74	5.64±0.50	0.12637±42

[1] This study, CT digestion, ID-ICP-MS (Re and PGE) and ID-TIMS (Os) techniques.
[2] Becker et al. (2006), CT digestion at 345°C in pressurized vessels, ID-ICP-MS (Re and PGE) and ID-TIMS (Os) techniques.
[3] Puchtel et al. (2005), CT digestion, ID-ICP-MS techniques.
[4] Meisel et al. (2003) and Meisel and Moser (2004), high pressure asher (HPA) digestion ID-ICP-MS (Re and PGE) and ID-TIMS (Os) techniques.
[5] Pearson et al. (2004), CT and HPA digestion ID-ICP-MS technique.
n – number of analyses. Errors quoted at $2\sigma_{mean}$

Table 2. Re-Os isotopic data for the Komati and Weltevreden Fm. whole-rock komatiite samples and olivine and chromite separates.

Sample	Re (ppb)	Os (ppb)	$^{187}Re/^{188}Os$	±2σ	$^{187}Os/^{188}Os$	±2σ	$\gamma^{187}Os(T)$
Komati Fm.							
BV02	0.0768	1.307	0.2830	0.0028	0.12028	0.00006	+0.36
BV05	0.0501	1.188	0.2030	0.0029	0.11540	0.00007	+0.26
BV08	0.0708	1.242	0.2745	0.0027	0.11964	0.00006	+0.23
BV09	0.1229	1.098	0.5400	0.0054	0.13579	0.00006	+0.51
BV01	0.1157	2.153	0.2585	0.0026	0.11872	0.00006	+0.26
BV03	0.0354	0.9443	0.1802	0.0018	0.11430	0.00005	+0.52
BV10	0.0410	1.263	0.1560	0.0016	0.11296	0.00006	+0.62
BV13	0.0217	1.827	0.0570	0.0066	0.10670	0.00006	+0.28
BV14	0.2745	1.6097	0.8216	0.0082	0.14461	0.00006	-7.3
BV15_A	0.0525	3.109	0.0812	0.0008	0.10793	0.00006	+0.08
BV15_B	0.0461	3.422	0.0648	0.0006	0.10745	0.00006	+0.56
BV15_IC_A*			0.0754	0.0008	0.10800	0.00006	+0.48
BV15_IC_A**					0.108038	0.000003	
BV15_IC_B*			0.0832	0.0008	0.10828	0.00006	+0.30
BV15_IC_B**					0.108284	0.000001	
BV16_A	0.1790	2.425	0.3555	0.0036	0.12450	0.00008	+0.25
BV16_B	0.1901	2.442	0.3756	0.0038	0.12584	0.00008	+0.39
BV16_IC*			0.3779	0.0038	0.12582	0.00008	+0.23
BV16_IC**					0.125851	0.000001	
BV03 Ol	0.0145	0.6612	0.1055	0.0030	0.10948	0.00007	+0.17
BV10 Ol	0.0033	0.3557	0.0452	0.0052	0.10569	0.00005	-0.01
BV03 Chr	0.2414	17.87	0.0649	0.0066	0.10714	0.00011	+0.26
BV10 Chr	0.2376	51.33	0.0222	0.0025	0.10484	0.00008	+0.50

Table 2. *(Continued)*

Sample	Re (ppb)	Os (ppb)	$^{187}Re/^{188}Os$	±2σ	$^{187}Os/^{188}Os$	±2σ	$\gamma^{187}Os(T)$
Weltevreden Fm.							
564-6	*0.317*	*1.238*	*1.242*	*0.012*	*0.17388*	*0.00009*	*-0.05*
501-3	*0.309*	*1.384*	*1.080*	*0.011*	*0.16486*	*0.00009*	*-0.03*
564-4	*0.331*	*0.9713*	*1.655*	*0.017*	*0.19693*	*0.00010*	*-0.09*
564-5	*0.284*	*1.457*	*0.9435*	*0.0094*	*0.15710*	*0.00009*	*-0.16*
12--2	*0.339*	*1.214*	*1.355*	*0.014*	*0.18025*	*0.00013*	*+0.01*
501-1_A	*0.153*	*10.77*	*0.0682*	*0.0007*	*0.10816*	*0.00005*	*-0.21*
501-1_B	0.143	10.11	0.0680	0.0007	0.10832	0.00006	-0.04
501-1_IC_A*			0.0660	0.0007	0.10808	0.00007	-0.16
501-1_IC_A**					0.107955	0.000002	
501-1_IC_B*			0.0670	0.0007	0.10809	0.00006	-0.21
501-1_IC_B**					0.108106	0.000001	
501-7	*0.258*	*1.074*	*1.158*	*0.006*	*0.14811*	*0.00007*	*-20.2*
501-8	0.183	0.9819	0.9023	0.0090	0.15474	0.00010	-0.22
501-9	*0.171*	*1.015*	*0.8122*	*0.0081*	*0.14979*	*0.00007*	*-0.15*
501-10	*0.162*	*6.621*	*0.1174*	*0.0012*	*0.11096*	*0.00005*	*-0.15*
501-10_IC*			0.1036	0.0010	0.11030	0.00005	-0.05
501-10_IC**					0.110303	0.000001	
427-5	0.159	7.354	0.1038	0.0010	0.11017	0.00005	-0.18
564-2	*0.141*	*2.660*	*0.2556*	*0.0026*	*0.11857*	*0.00006*	*-0.26*
564-3	*0.0664*	*3.066*	*0.1042*	*0.0010*	*0.11024*	*0.00005*	*-0.14*
12--6	*0.162*	*4.345*	*0.1794*	*0.0018*	*0.11452*	*0.00007*	*-0.06*
12--7	0.175	5.089	0.1656	0.0017	0.11360	0.00007	-0.20
12--8	*0.122*	*4.699*	*0.1246*	*0.0012*	*0.11139*	*0.00005*	*-0.12*
12--8_IC*			0.1254	0.0013	0.11146	0.00006	-0.10
12--8_IC**					0.111500	0.000001	
501-1 Ol	*0.0184*	*8.552*	*0.0103*	*0.0003*	*0.10501*	*0.00005*	*-0.13*
501-8 Ol	0.0033	2.385	0.0067	0.0010	0.10483	0.00007	-0.10
12-6 Ol	0.0029	3.321	0.0042	0.0007	0.10467	0.00007	-0.13

Note. The initial $\gamma^{187}Os$ were calculated for the ages ***T*** defined by the isochrons for the Komati (3484 Ma) and Weltevreden (3263 Ma) komatiite systems using the model parameters specified in the text. Italicized values represent data from Connolly et al. (2011) reported here for convenience.

(*) Averages for the spiked aliquots of the unspiked digestions processed for the Pt-Os study (see **Table 3**) to determine the Re/Os and Pt/Os ratios.

(**) Data from the high-precision runs for the Pt-Os study (see **Table 3**). These data are shown here for comparison with the data for the spiked runs only and were not used for the isochron calculations.

Table 3. High-precision osmium isotopic data and Re/Os and Pt/Os ratios for the Komati and Weltevreden komatiite systems.

Sample	$^{187}Re/^{188}Os$	$^{190}Pt/^{188}Os$	$^{184}Os/^{188}Os$	$^{186}Os/^{188}Os$	$^{187}Os/^{188}Os$	$\varepsilon^{186}Os(T)$	$\gamma^{187}Os(T)$
Komati Fm.							
BV15_A	0.0754	0.001021	0.001316±4	0.1198336±25	0.1080382±29	-0.12±0.21	+0.52
BV15_B	0.0832	0.001172	0.001310±1	0.1198344±9	0.1082836±13	-0.11±0.07	+0.30
BV16	0.378	0.001205	0.001307±1	0.1198343±7	0.1258510±09	-0.13±0.06	+0.26
Weltevreden Fm.							
501-1_A	0.0660	0.000337	0.001306±7	0.1198344±11	0.1079550±24	+0.21±0.10	-0.28
501-1_B	0.0670	0.000334	0.001312±5	0.1198346±21	0.1081057±13	+0.22±0.18	-0.19
501-10	0.104	0.000556	0.001305±2	0.1198354±18	0.1103029±09	+0.20±0.15	-0.05
12-8	0.125	0.000800	0.001302±3	0.1198373±9	0.1114998±13	+0.26±0.08	-0.06

Note. The uncertainties on the Re/Os and Pt/Os ratios are 1.0% relative. The initial $\varepsilon^{186}Os$ and $\gamma^{187}Os$ values were calculated for the emplacement ages of 3484 Ma (Komati Fm.) or 3263 Ma (Weltevreden Fm.) defined by the respective Re-Os isochrons.

Table 4. Highly siderophile element abundance data (ppb) for the Komati and Weltevreden Fm. whole-rock komatiite samples and mineral separates.

Sample	Re	Os	Ir	Ru	Pt	Pd	$(Os/Ir)_N$	$(Pd/Ir)_N$
Komati system. ***Chilled margin***								
BV02	0.0818	1.391	1.34	3.53	5.00	4.62	**1.01**	**2.70**
Olivine spinifex								
BV05	0.0532	1.262	1.40	3.72	5.29	4.98	**0.88**	**2.79**
BV08	0.0754	1.322	1.42	3.71	4.84	4.77	**0.90**	**2.63**
BV09	0.129	1.148	1.31	3.51	5.93	5.77	**0.85**	**3.45**
Olivine cumulates								
BV01	0.124	2.315	2.03	3.68	4.06	3.99	**1.11**	**1.54**
BV03	0.0374	0.9990	0.979	3.13	3.26	3.49	**0.99**	**2.78**
BV10	0.0438	1.352	1.20	3.56	3.33	3.55	**1.09**	**2.31**
BV13	0.0233	1.965	1.78	4.90	3.21	3.21	**1.07**	**1.41**
BV14	0.296	1.736	1.69	6.75	4.01	4.20	**1.00**	**1.94**
BV15	0.0563	3.333	2.95	4.36	3.40	3.51	**1.10**	**0.93**
Replicate	0.0495	3.669	3.09	4.33	3.40	3.49	**1.15**	**0.88**
BV16	0.192	2.603	2.46	4.36	3.84	3.79	**1.03**	**1.21**
Replicate	0.204	2.622	2.50	4.65	3.81	3.94	**1.02**	**1.23**
Olivine and chromite separates								
BV03 Ol	0.0145	0.6612	0.608	2.72	0.268	0.400	**1.05**	**0.51**
BV10 Ol	0.0034	0.3557	0.363	2.69	0.0800	0.0813	**0.95**	**0.17**
BV03 Chr	0.241	17.87	20.5	236	6.21	4.10	**0.84**	**0.16**
BV10 Chr	0.238	51.33	51.9	400	6.69	1.22	**0.96**	**0.018**

Table 4. (Continued).

Sample	Re	Os	Ir	Ru	Pt	Pd	$(Os/Ir)_N$	$(Pd/Ir)_N$
Weltevreden system. ***Chilled margin***								
564-6	*0.345*	*1.35*	*1.40*	*6.55*	*9.10*	*7.04*	***0.90***	***3.37***
Olivine spinifex								
501-3	*0.333*	*1.49*	*1.56*	*5.94*	*8.58*	*6.60*	***0.90***	***2.85***
564-4	*0.357*	*1.05*	*1.13*	*6.25*	*9.52*	*7.46*	***0.87***	***4.45***
564-5	*0.308*	*1.58*	*1.57*	*6.14*	*8.43*	*6.65*	***0.94***	***2.84***
12-2	*0.366*	*1.31*	*1.40*	*6.54*	*9.60*	*7.56*	***0.88***	***3.62***
Olivine cumulate								
501-1	*0.170*	*11.9*	*10.6*	*6.32*	*4.35*	*3.33*	***1.05***	***0.21***
Replicate	0.159	11.3	9.23	6.67	4.45	3.15	**1.14**	**0.23**
501-7	*0.284*	*1.18*	*1.10*	*5.48*	*4.98*	*3.98*	***1.01***	***2.42***
501-8	0.201	1.08	1.12	6.07	4.90	3.52	**0.90**	**2.11**
501-9	*0.187*	*1.11*	*1.05*	*5.29*	*4.74*	*3.67*	***1.00***	***2.35***
501-10	*0.173*	*7.07*	*6.00*	*5.49*	*4.53*	*3.53*	***1.11***	***0.40***
427-5	0.175	8.10	6.51	5.68	4.64	3.31	**1.17**	**0.34**
564-2	*0.154*	*2.89*	*2.92*	*9.06*	*4.37*	*3.34*	***0.93***	***0.77***
564-3	*0.0720*	*3.32*	*3.42*	*8.98*	*4.55*	*3.32*	***0.91***	***0.65***
12-6	*0.177*	*4.75*	*4.35*	*6.12*	*4.75*	*3.78*	***1.02***	***0.58***
12-7	0.194	5.65	4.83	6.12	4.69	3.33	**1.10**	**0.46**
12-8	*0.134*	*5.18*	*4.84*	*6.66*	*4.29*	*3.23*	***1.01***	***0.45***
Olivine separates								
501-1 Ol	*0.0184*	*8.55*	*7.42*	*5.92*	*0.701*	*0.457*	***1.08***	***0.041***
501-8 Ol	0.0033	2.39	2.18	7.11	0.129	0.0789	**1.03**	**0.024**
12-6 Ol	0.0029	3.32	2.92	6.51	0.441	0.0794	**1.07**	**0.018**

Note. Abundances are re-calculated on an anhydrous basis. Italicized values represent data from Connolly et al. (2011) reported here for convenience. The Os/Ir and Pd/Ir ratios are normalized relative to average Orgueil values from Horan et al. (2003).

Table 5. Calculated HSE abundances (ppb) in the emplaced lavas and mantle sources of the Komati and Weltevreden komatiite systems.

	Re	**Os**	**Ir**	**Ru**	**Pt**	**Pd**	**$(Os/Ir)_N$**	**$(Pd/Ir)_N$**
Komati system								
Emplaced lava		1.3±0.1	1.4±0.1	3.6±0.2	4.8±0.4	4.7±0.4	0.93±0.05	2.7±0.2
Source	0.29±0.10	3.3±1.1	3.5±1.2	3.5±0.3	2.9±0.2	2.9±0.2	0.93±0.33	0.83±0.29
Source Pt-corrected	0.29±0.10	3.3±1.1	3.5±1.2	3.5±0.3	5.9±0.9	2.9±0.2	0.93±0.33	0.83±0.29
Weltevreden system								
Emplaced lava	0.33±0.03	1.4±0.1	1.5±0.1	6.3±0.2	8.5±0.5	6.6±0.5	0.94±0.08	3.5±0.2
Source	0.23±0.02	2.7±0.2	2.9±0.3	6.0±0.3	6.0±0.4	4.6±0.3	0.94±0.08	1.6±0.1
Source Pt-corrected	0.23±0.02	2.7±0.2	2.9±0.3	6.0±0.3	4.9±0.7	4.6±0.3	0.94±0.08	1.6±0.1

Note. Re abundances in the emplaced Komati lava could not be calculated due to Re post-emplacement mobility.

Figure(s)

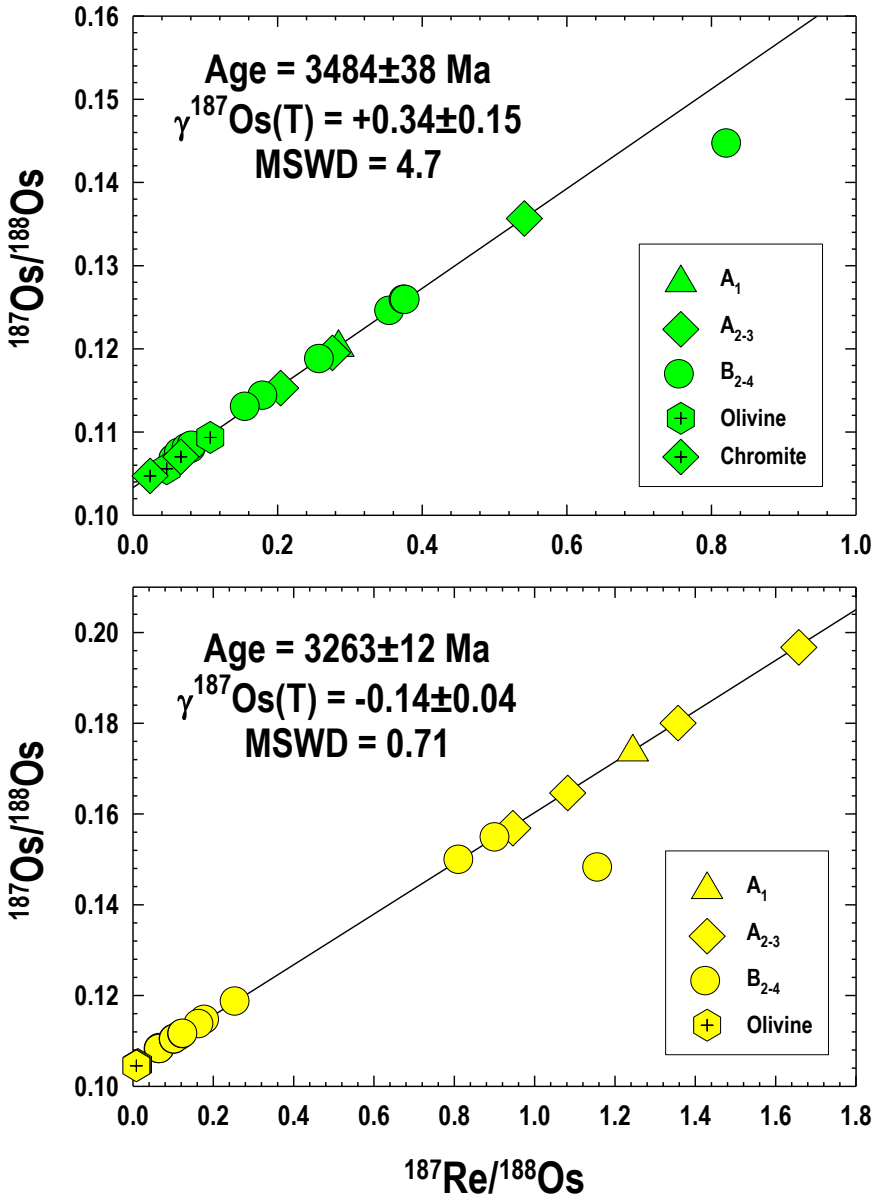

Figure 1.

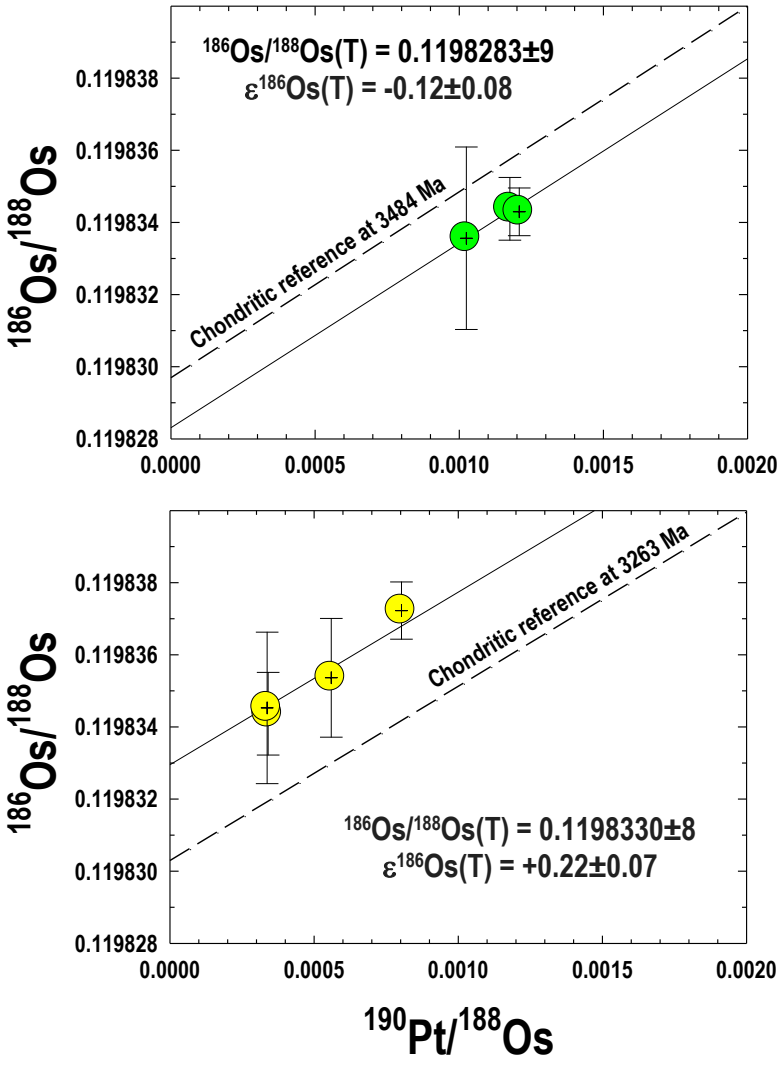
$^{186}Os/^{188}Os(T) = 0.1198283\pm9$
$\varepsilon^{186}Os(T) = -0.12\pm0.08$
Chondritic reference at 3484 Ma
$^{186}Os/^{188}Os(T) = 0.1198330\pm8$
$\varepsilon^{186}Os(T) = +0.22\pm0.07$
Chondritic reference at 3263 Ma
$^{186}Os/^{188}Os$
$^{190}Pt/^{188}Os$
0.119828
0.119830
0.119832
0.119834
0.119836
0.119838
0.0000
0.0005
0.0010
0.0015
0.0020

Figure 2.

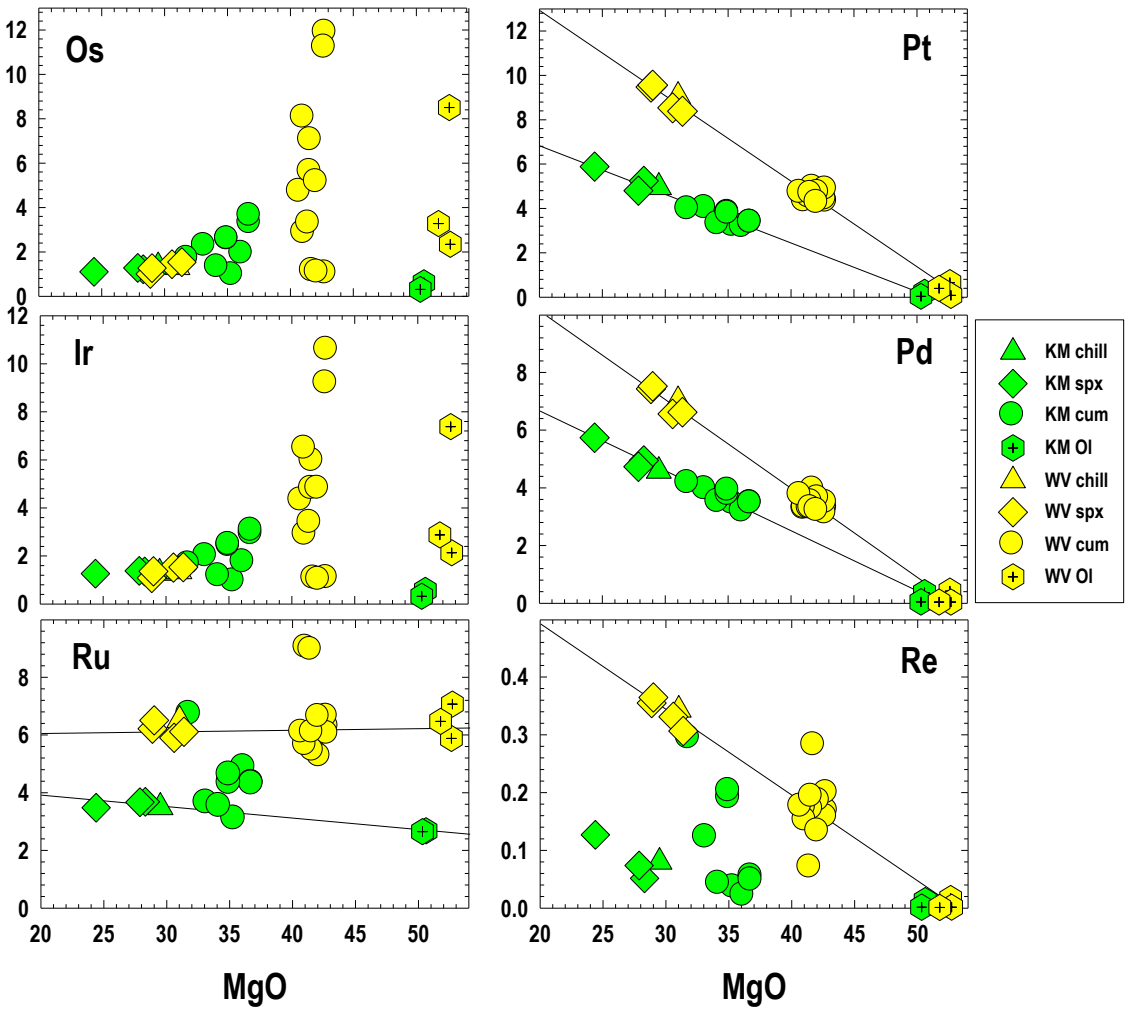
Os
Pt
Ir
Pd
Ru
Re
MgO
MgO
KM chill
KM spx
KM cum
KM Ol
WV chill
WV spx
WV cum
WV Ol

Figure 3.

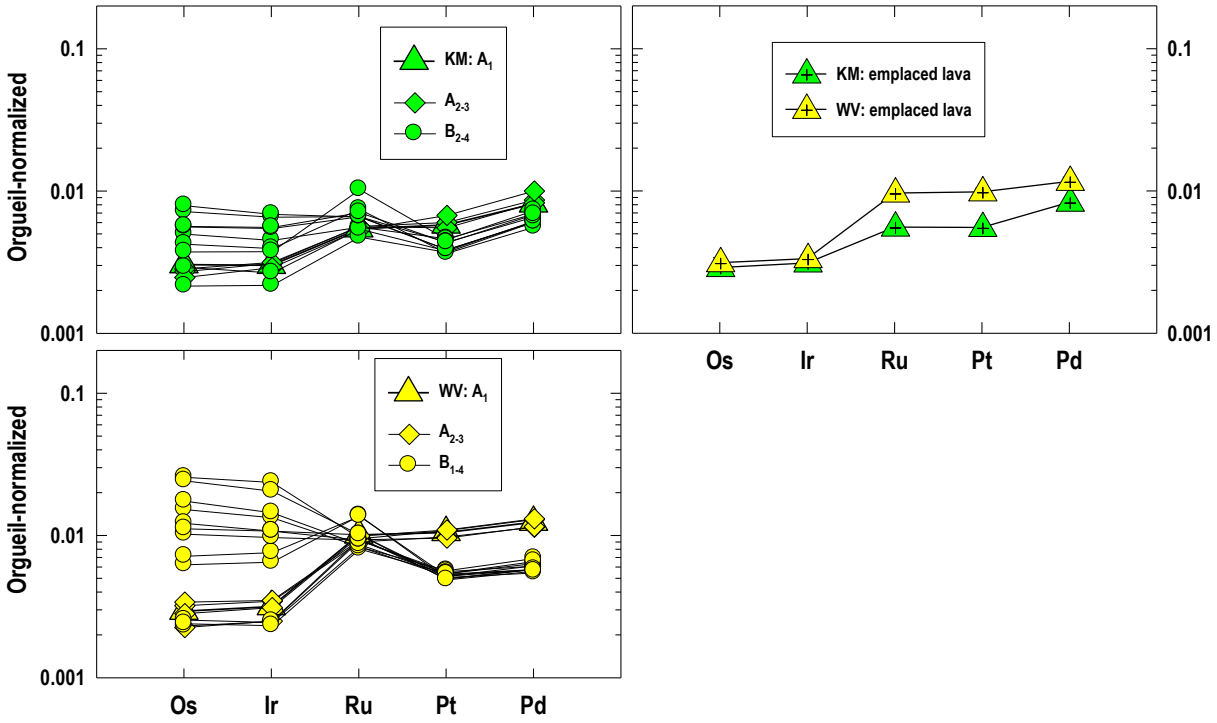
Orgueil-normalized
0.1
0.01
0.001
KM: A1
A2-3
B2-4
KM: emplaced lava
WV: emplaced lava
WV: A1
A2-3
B1-4
Os
Ir
Ru
Pt
Pd

Figure 4.

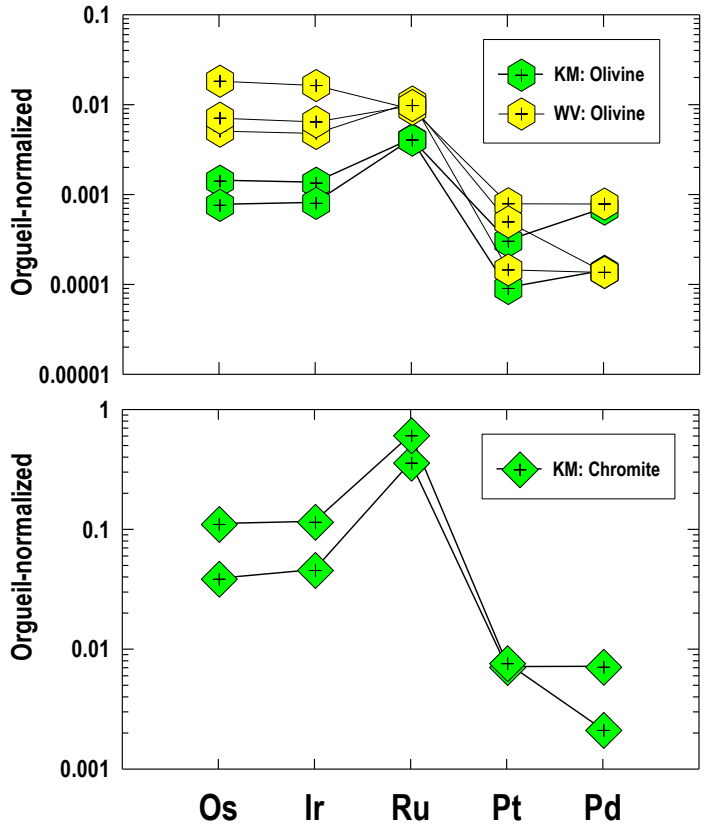
0.1
0.01
0.001
0.0001
0.00001
Orgueil-normalized
KM: Olivine
WV: Olivine
1
0.1
0.01
0.001
Orgueil-normalized
KM: Chromite
Os
Ir
Ru
Pt
Pd

Figure 5.

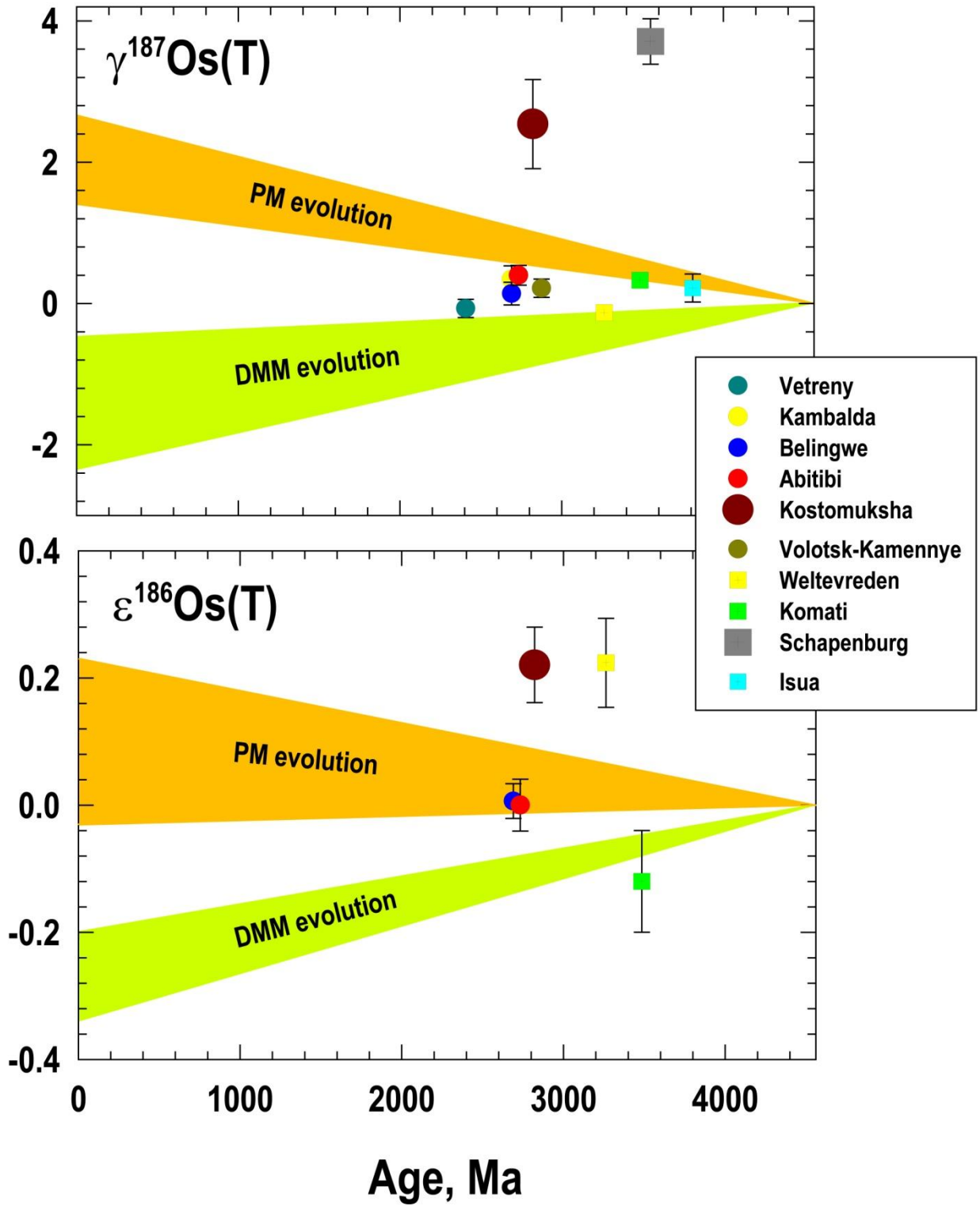
γ187Os(T)
PM evolution
DMM evolution
ε186Os(T)
PM evolution
DMM evolution
Vetreny
Kambalda
Belingwe
Abitibi
Kostomuksha
Volotsk-Kamennye
Weltevreden
Komati
Schapenburg
Isua
4
2
0
-2
0.4
0.2
0.0
-0.2
-0.4
0
1000
2000
3000
4000
Age, Ma

Figure 6.

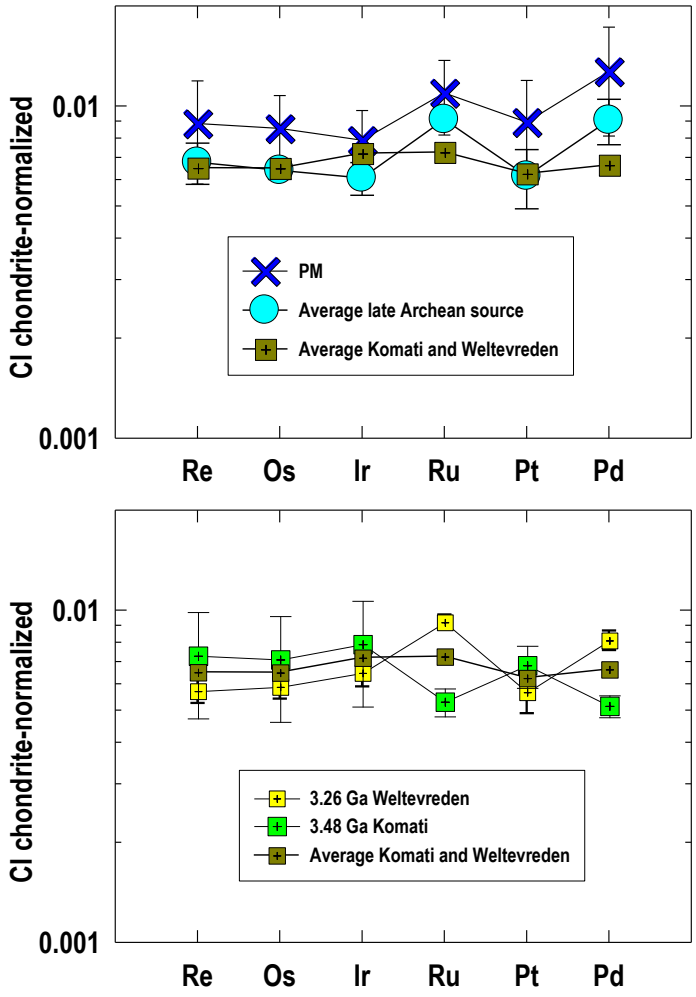
Cl chondrite-normalized
0.01
0.001
Re
Os
Ir
Ru
Pt
Pd
PM
Average late Archean source
Average Komati and Weltevreden
Cl chondrite-normalized
0.01
0.001
Re
Os
Ir
Ru
Pt
Pd
3.26 Ga Weltevreden
3.48 Ga Komati
Average Komati and Weltevreden

Figure 7.

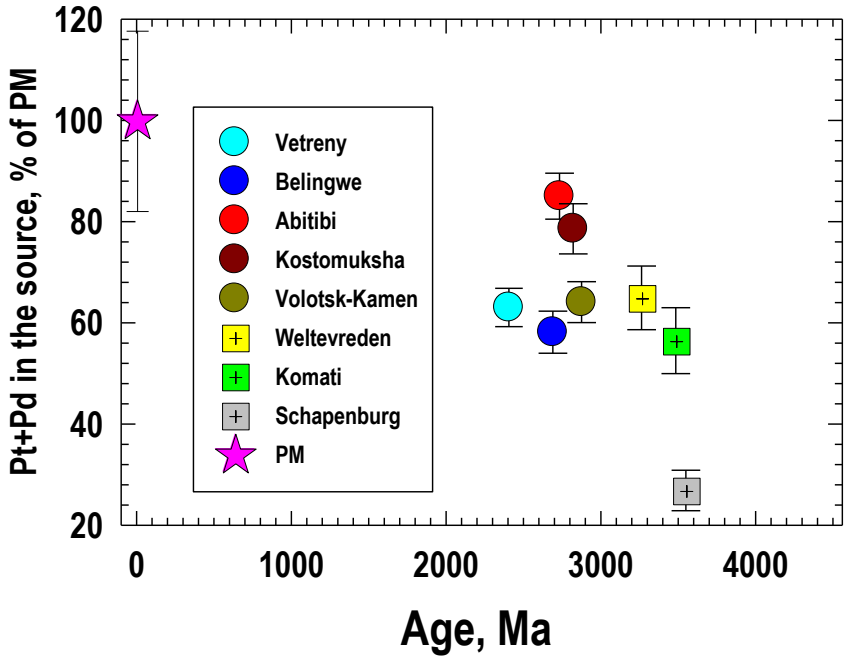
Pt+Pd in the source, % of PM
120
100
80
60
40
20
0
1000
2000
3000
4000
Age, Ma
Vetreny
Belingwe
Abitibi
Kostomuksha
Volotsk-Kamen
Weltevreden
Komati
Schapenburg
PM

Figure 8.